Atmospheric
Chemistry
and Physics

Measurement report: Contribution of atmospheric new particle formation to ultrafine particle concentration, cloud condensation nuclei, and radiative forcing – results from 5-year observations in central Europe

Jia Sun[1,2], Markus Hermann[2], Kay Weinhold[2], Maik Merkel[2], Wolfram Birmili[3], Yifan Yang[2],
Thomas Tuch[2], Harald Flentje[4], Björn Briel[4], Ludwig Ries[3], Cedric Couret[3], Michael Elsasser[3],
Ralf Sohmer[3], Klaus Wirtz[3], Frank Meinhardt[3], Maik Schütze[3], Olaf Bath[3], Bryan Hellack[3],
Veli-Matti Kerminen[5], Markku Kulmala[5], Nan Ma[6], and Alfred Wiedensohler[2]

[1]Southern Marine Science and Engineering Guangdong Laboratory (Guangzhou), Guangzhou, 511458, China
[2]Atmospheric Microphysics Department, Leibniz Institute for Tropospheric Research (TROPOS),
Leipzig, Germany
[3]German Environment Agency (UBA), Berlin, Germany
[4]Deutscher Wetterdienst (DWD), Meteorologisches Observatorium Hohenpeißenberg,
Hohenpeißenberg, Germany
[5]Department of Physics, University of Helsinki, P.O. Box 64, 00014 Helsinki, Finland
[6]College of Environment and Climate, Institute for Environmental and Climate Research,
Guangdong-Hongkong-Macau Joint Laboratory of Collaborative Innovation for Environmental Quality, Jinan
University, Guangzhou, Guangdong, 511443, China

Correspondence: Nan Ma (nan.ma@jnu.edu.cn) and Alfred Wiedensohler (ali@tropos.de)

Abstract. As an important source of sub-micrometer particles, atmospheric new particle formation (NPF) has been observed in various environments. However, most studies provide little more than snapshots of the NPF process due to their underlying observations being limited in space and time. To obtain statistically relevant evidence on NPF across various environments, we investigated the characteristics of NPF based on a 5-year dataset of the German Ultrafine Aerosol Network (GUAN). The results were also compared with observations in previous studies, with the aim to depict a relatively complete picture of NPF in central Europe. The highest NPF occurrence frequency was observed in regional background sites, with an average of about 19 %, followed by urban background (15 %), low-mountain-range (7 %), and high Alpine (3 %) sites. The annual mean growth rate between 10 and 25 nm varied from 3.7–4.7 nm h^{-1}, while the formation rate with same size range 10–25 nm from 0.4 to 2.9 cm^{-3} s^{-1}. The contribution of NPF to ultrafine particles (UFPs) was about 13 %, 21 %, and 7 % for the urban background, regional background, and low mountain range, respectively. The influence of NPF on cloud condensation nuclei (CCN) number concentration and the aerosol extinction coefficient for NPF days was the highest in mountainous areas. These findings underscore the importance of local environments when assessing the potential impact of NPF on regional climate in models, and they also emphasize the usefulness of a long-term aerosol measurement network for understanding the variation in NPF features and their influencing factors over a regional scale.

1 Introduction

Atmospheric new particle formation (NPF) is a process initiated with the sudden formation of new particles with diameters of less than 3 nm in the atmosphere. Low-volatility gas molecules oxidated from gas-phase precursors cluster together and form new aerosol particles. These nanoparticles may subsequently grow into larger sizes by condensation or coagulation (Kulmala et al., 2014). The newly formed aerosol particles have the potential to contribute greatly to the number concentration of ultrafine particles (UFPs, particles smaller than 100 nm) or even larger sub-micrometer particles (particles smaller than 1 µm) (Ma and Birmili, 2015). Once the newly formed particles grow into larger sizes (typically more than 100 nm), they can affect cloud properties and processes by acting as cloud condensation nuclei (CCN) (Dameto De España et al., 2017; Hirshorn et al., 2022; Ren et al., 2021; Williamson et al., 2019). As an essential source of atmospheric aerosols, NPF events can also impact the regional radiative forcing of the atmosphere by increasing the overall extinction of light as the particles grow larger (Shen et al., 2011).

NPF is a complex process affected by various factors, including meteorological conditions (Bousiotis et al., 2021a; Li et al., 2019; Salvador et al., 2021), atmospheric chemical composition (Dada et al., 2020; Dall'Osto et al., 2018; Németh et al., 2018; Nieminen et al., 2014), and pre-existing aerosol loading (Bousiotis et al., 2021b; Salma and Németh, 2019). Studies on NPF have been conducted in diverse environments, ranging from polluted megacities (Yao et al., 2018; Wang et al., 2014) to clean areas (Petäjä et al., 2009; Vana et al., 2016). Experimental observations show that in the continental boundary layer, NPF often occurs in the shape of "NPF events"; i.e., the nucleation and subsequent growth of particles may take place over horizontal spatial scales that are up to several tens or hundreds of kilometers. Such "banana"-type NPF events with particle formation and growth can accordingly occur across various locations and diverse types of environments (Kerminen et al., 2018). The basis of experimental observations has grown steadily over the past 30 years, and a plethora of computational models have been developed to describe NPF on mechanistic and empirical levels.

However, the conclusions drawn from existing studies show large discrepancies, and the influence of local atmospheric or meteorological conditions on NPF has not been fully understood yet. For instance, although some studies have reported that environments of low ambient relative humidity (RH) favor NPF (Cai et al., 2017; Dada et al., 2017; Li et al., 2019), NPF has still been observed in environments with high RH (O'Dowd et al., 1998; Bousiotis et al., 2021b). High temperature associated with strong solar radiation can promote photochemical reaction and nucleation (Boy and Kulmala, 2002; Kürten et al., 2016; Ma and Birmili, 2015), and well-mixed air leads to a low condensation sink (CS),

resulting in a higher probability of NPF (Größ et al., 2018; Dall'Osto et al., 2018; Bousiotis et al., 2021a). Conversely, high temperature and well-mixed atmosphere may also inhibit NPF by decreasing the stability of molecular clusters (Hanson et al., 2017; Kürten et al., 2018). Additionally, the role of mixed atmospheric chemical species, including SO_2, NH_3, and volatile organic compounds (VOCs), is complex and varies with the nucleation mechanism and concentration of those components (Laaksonen et al., 2008; Ehn et al., 2014; Kürten et al., 2016; Qi et al., 2018). To understand the characteristics of NPF and its influencing factors, field campaign experiments covering a wide range of atmospheric conditions and environments are essential (Lee et al., 2019).

Continuous observations of NPF started as single-point observations at ground level (Mäkelä et al., 1997; Birmili and Wiedensohler, 2000) and were subsequently expanded to cover greater spatial and temporal scales. Several studies have investigated NPF at multiple sites at the small-region scale (for example around a city) (Costabile et al., 2009; Németh and Salma, 2014; Bousiotis et al., 2019; Casquero-Vera et al., 2020; Kalkavouras et al., 2020; Smejkalova et al., 2021; etc.), at the country or continent scale (Manninen et al., 2010; Dall'Osto et al., 2018; Németh et al., 2018; Bousiotis et al., 2021a; Sebastian et al., 2022; etc.), and at the global scale (Ren et al., 2021; Nieminen et al., 2018; Sellegri et al., 2019). Small-region-scale studies refer to individual NPF observations within regional and closer distances (< 200 km), such as in central France (Boulon et al., 2011), Budapest (Németh and Salma, 2014; Salma et al., 2017), the southern UK (Bousiotis et al., 2019), and Leipzig (Ma and Birmili, 2015). These studies have mainly focused on the difference in NPF features with varying degrees of anthropogenic and biogenic emissions (Ma and Birmili, 2015; Bousiotis et al., 2019) or the characteristics of NPF events occurring simultaneously at several sites in a small area (Németh and Salma, 2014; Salma et al., 2016). Country-based or continental-scale studies can provide insight into the connection between NPF events and their influencing factors covering a particular region, such as Europe (Dall'Osto et al., 2018; Bousiotis et al., 2021b; Manninen et al., 2010) and India (Sebastian et al., 2022). Global analyses of NPF events stretch these comparisons further, comparing the characteristics of NPF under one environment (Sellegri et al., 2019) or multiple types of environments (Nieminen et al., 2018; Ren et al., 2021). However, comprehensive observations of regional NPF across multiple sites have still been limited to date, with most studies including only two or three sites, leading to open questions when explaining the spatial and temporal variabilities in regional NPF across diverse environments throughout a large region.

The German Ultrafine Aerosol Network (GUAN) is an observation network for sub-micrometer aerosol particle measurements, aiming at a better understanding of the associated climate and health effects. GUAN provides long-term atmospheric aerosol measurements in diverse site categories in Germany, ranging from roadside to high Alpine areas (Bir-
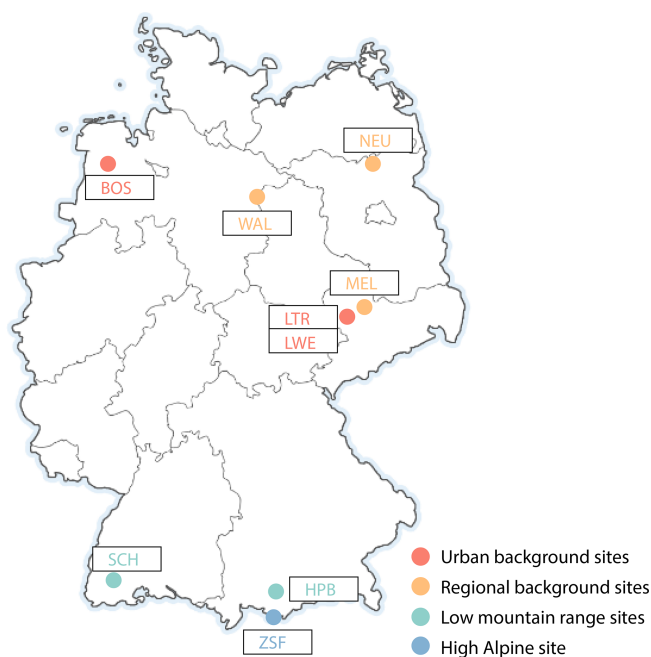
Figure 1. The locations of the nine selected observation sites in the German Ultrafine Aerosol Network (GUAN).

mili et al., 2016; Sun et al., 2020). On the basis of the GUAN observations, a comprehensive comparison of NPF in various environments across Germany is realistic. Based on a 5-year dataset, we investigated the characteristics of NPF for various environments from urban background to high Alpine, including the occurrence of NPF events, particle formation, and growth rates, and the impacts of NPF on UFPs, CCN, and radiative forcing, aiming to depict a relatively complete picture of NPF in central Europe.

2 Measurement and data

2.1 Measurement sites

This study uses atmospheric observations from nine observation sites in the German Ultrafine Aerosol Network (GUAN; Birmili et al., 2016). GUAN is a cooperative observation network of several research organizations that has provided continuous measurement of sub-micrometer particle number size distributions (PNSDs) and equivalent black carbon (eBC) mass concentration since 2009. GUAN consists of 17 measurement sites covering diverse environmental settings in Germany including roadside, urban background (UB), regional background (RB), low-mountain-range (LMT), and high Alpine (HA). The locations and characteristics of the nine selected measurement sites are shown in Fig. 1 and Table 1. For a detailed description, see Birmili et al. (2016).

The nine GUAN measurement sites in this study comprise three UB sites, three RB sites, two LMT sites, and one HA site. The three UB sites are Leipzig-West (LWE), the Leib-

niz Institute for Tropospheric Research (TROPOS) (LTR), and Bösel (BOS). LWE and LTR are both located in the city of Leipzig, 10 km apart. LTR is situated on the roof of the main TROPOS building, while LWE is situated in a hospital park in the western suburbs of Leipzig. BOS is located in the village of Bösel, about 100 km away from the North Sea.

The RB site Melpitz (MEL) is about 50 km northeast of Leipzig. Its surroundings are flat and seminatural grasslands without significant anthropogenic sources. The Neuglobsow (NEU) and Waldhof (WAL) sites are situated in northern German forest regions. A previous study showed that MEL can represent the regional background atmosphere of central Europe (Spindler et al., 2013), while NEU and WAL represent the regional background conditions in the northern German lowlands (Sun et al., 2019).

Three mountainous sites in GUAN are located in southern Germany, including two LMT sites, Schauinsland (SCH, 1205 m a.s.l.) and Hohenpeißenberg (HPB, 980 m a.s.l.), and one HA site, Zugspitze Schneefernerhaus (ZSF, 2670 m a.s.l.). SCH is situated in the Black Forest, and HPB is on a solitary hill in the countryside of southern Bavaria, 40 km north of the Alpine mountain range and 45 km southwest of the Munich region. As a part of the World Meteorological Organization (WMO) Global Atmosphere Watch (GAW) program, ZSF is located on the south side of Zugspitze Mountain, approximately 300 m below the summit, and the air masses of both the lower free troposphere (FT) and the planetary boundary layer (PBL) can be observed there (Sun et al., 2021; Yuan et al., 2019).

2.2 Instrumentation

Aerosol PNSDs were measured by either mobility particle size spectrometer (MPSS; Wiedensohler et al., 2012) or dual mobility particle size spectrometer (D-MPSS). Some stations used an additional thermodenuder option, thermodenuder mobility particle size spectrometer (TDMPSS; Wang et al., 2017), whose data, however, were not used in this analysis. The specifications of the instruments used at each site are summarized in Table 1. To ensure standardized conditions for particle sizing at different sites and times, PNSDs were generally measured in a dry state with RH below 40 % (Swietlicki et al., 2008). An inversion algorithm developed by Pfeifer et al. (2014) based on bipolar charge distribution (Wiedensohler, 1988) was used to retrieve the PNSD from the measured raw mobility distribution. The particle losses in instruments and inlet systems were corrected based on Wiedensohler et al. (2012), and the quality assurance (QA) was performed as described in Wiedensohler et al. (2018).

The QA of MPSS measurements in GUAN, including both instrument-to-instrument and instrument-to-standard comparisons, was regularly conducted by the World Calibration Centre for Aerosol Physics (WCCAP; http://www.wmo-gaw-wcc-aerosol-physics.org/, last access: 12 April 2023) in Leipzig. The aim of QA is to obtain an ac-

Table 1. Information about the nine GUAN sites and the corresponding PNSD measurements, in alphabetical order.

No.	Site name	Abbreviation	Site category	Altitude	Location	MPSS type	Size range
1.	Bösel	BOS	Urban background	17 m	52°59′53″ N, 07°56′34″ E	MPSS	10–800 nm
2.	Hohenpeißenberg	HPB	Low-mountain-range	980 m	47°48′06″ N, 11°00′34″ E	MPSS	10–800 nm
3.	Leipzig-TROPOS	LTR	Urban background	126 m	51°21′10″ N, 12°26′03″ E	TDMPSS	5–800 nm
4.	Leipzig-West	LWE	Urban background	122 m	51°19′05″ N, 12°17′51″ E	TDMPSS	10–800 nm
5.	Melpitz	MEL	Regional background	86 m	51°31′32″ N, 12°55′40″ E	D-MPSS	5–800 nm
6.	Neuglobsow	NEU	Regional background	70 m	53°08′28″ N, 13°01′52″ E	MPSS	10–800 nm
7.	Schauinsland	SCH	Low-mountain-range	1205 m	47°54′49″ N, 07°54′29″ E	MPSS	10–800 nm
8.	Waldhof	WAL	Regional background	75 m	52°48′04″ N, 10°45′23″ E	MPSS	10–800 nm
9.	Zugspitze Schneefernerhaus	ZSF	High Alpine	2670 m	47°25′00″ N, 10°58′47″ E	MPSS (TSI 3936)	20–600 nm

curacy within a few percent for the particle sizing and $\pm 10\%$ for the particle number concentration (PNC) of PNSD over the entire measurement period. The periodical QA procedures for MPSSs include daily or weekly inspection and monthly and annual full maintenance, either at the measurement site or at the laboratory of WCCAP. Detailed descriptions of the QA procedure are given in Birmili et al. (2016).

The PNSD data used in this study cover a 5-year period from 2009–2013, with three exceptions: NEU and LWE started PNSD measurements in 2011 and the PNSD data at ZSF are available from 2012. The temporal coverage of quality-checked PNSD data at the nine sites is given in Fig. S1 in the Supplement.

2.3 Method

2.3.1 NPF event classification

The classification of NPF events was performed visually according to the criteria given by Dal Maso et al. (2005). If a distinct new nucleation mode (3–25 nm) appeared and grew into the Aitken-mode size range (25–100 nm) within the subsequent hours between 00:00 and 24:00 local time, such a day was classified as an NPF day. The NPF event was classified as type I if the formation and growth rate of the NPF event could be clearly determined from the observed evolution of the PNSD and as type II otherwise. The formation and growth rates were calculated only for type I events. Type

I events were further grouped into two sub-classes: Ia and Ib. Type Ia contains very strong and clear NPF with a banana shape, and the rest of the type I events were classified as type Ib. The days were classified as "undefined events" if the cases could not be clearly classified as events or non-events.

2.3.2 Calculation of growth, formation rates, and the condensation sink

The growth and formation rate were evaluated for type I events in this study, while the condensation sink (CS) was evaluated for all NPF events. The growth rate of nucleation-mode particles (GR_{10-25}) is defined as the change rate of the modal diameter of the newly formed particles (Kulmala et al., 2012):

$$GR_{10-25} = \left(D_{P_2} - D_{P_1}\right)/\left(t_2 - t_1\right), \tag{1}$$

where D_{P_1} and D_{P_2} are the geometric mean diameters (GMDs) of the mode of newly formed particles at the start and end time during an NPF event. The GMDs were obtained by the log-normal modal fitting of the PNSD.

The formation rate in nucleation mode (J_{10-25}) is the sum of the increase rate, the decrease rate of N_{10-25} due to coagulation losses, and the decrease rate of N_{10-25} due to condensational growth out of the nucleation mode. Accordingly, J_{10-25} was obtained using the following equation (Kulmala

et al., 2012):

$$J_{10-25} = \frac{\mathrm{d}N_{10-25}}{\mathrm{d}t} + \mathrm{CoagS}_{10\,\mathrm{nm}} \times N_{10-25}$$
$$+ \frac{\mathrm{GR}_{10-25}}{\Delta D_{\mathrm{p}}} \times N_{10-25}, \quad (2)$$

where $\mathrm{CoagS}_{10\,\mathrm{nm}}$ is the coagulation sink of particles with a diameter of 10 nm. This can be calculated using the method proposed by Kerminen et al. (2001):

$$\mathrm{CoagS}_{10\,\mathrm{nm}} = \sum_{D'_{\mathrm{p}}=10\,\mathrm{nm}}^{D'_{\mathrm{p}}=800\,\mathrm{nm}} K(10\,\mathrm{nm}, D'_{\mathrm{p}}) N_{D'_{\mathrm{p}}}, \quad (3)$$

where $K(10\,\mathrm{nm}, D'_{\mathrm{p}})$ is the coagulation coefficient between particles with sizes of 10 nm and D'_{p} and $N_{D'_{\mathrm{p}}}$ is the particle number concentration of particles with size D'_{p}.

CS describes how fast the condensable vapor molecules condense on the pre-existing aerosol particles (Dal Maso et al., 2002), which can be obtained from

$$\mathrm{CS} = 2\pi D \sum_{i} \beta_i d_{pi} N_i, \quad (4)$$

where D is the diffusion coefficient of the vapor, calculated based on the properties of sulfuric acid; d_{pi} is the diameter of a particle in size class i; and N_i is the particle number concentration in the respective size class. β_i is the transition regime correction factor:

$$\beta_i = \frac{1 + Kn}{1 + \left(\frac{4}{3\alpha_i} + 0.337\right) Kn + \frac{4}{3\alpha} Kn^2}, \quad (5)$$

where α is the accommodation coefficient for mass transfer, which is assumed to be unity in our calculations. Kn is the Knudsen number:

$$Kn = 6\sqrt{\frac{\pi m}{8k_{\mathrm{b}}T}} D, \quad (6)$$

where m is the mass of a vapor molecule, T is temperature, and k_{b} is the Boltzmann constant.

2.3.3 Nucleation strength factor

The nucleation strength factor (NSF) proposed by Németh and Salma (2014) qualitatively evaluates the overall concentration increment on NPF days exclusively, calculated by

$$\mathrm{NSF_{nuc}} = \frac{(N_{10-100}/N_{100-800})_{\text{all NPF event days}}}{(N_{10-100}/N_{100-800})_{\text{all non-event days}}}. \quad (7)$$

2.3.4 Contribution to UFP number concentration

The contribution of NPF to UFP number concentration was quantitatively estimated by segregating the diurnal patterns of UFPs driven by NPF, urban sources, and the regional background (Ma and Birmili, 2015). Like Ma and Birmili (2015),

we observed that, in Germany, NPF events occurred almost exclusively on days with a daily average solar radiation of more than $100\,\mathrm{W\,m^{-2}}$. Subsequently, the measurement period was first separated into high-solar-radiation and low-solar-radiation days by a threshold of daily average solar radiation of $100\,\mathrm{W\,m^{-2}}$, to accurately estimate the effect of NPF to UFP number concentration. The average diurnal cycles of UFP number concentration for NPF days and non-event days in the high-solar-radiation period were calculated and denoted $\tilde{N}_{\mathrm{HR\text{-}NPF}}$ and $\tilde{N}_{\mathrm{HR\text{-}NON}}$, respectively. Similarly, the corresponding values in the low-solar-radiation period were calculated and denoted $\tilde{N}_{\mathrm{LR\text{-}NPF}}$ and $\tilde{N}_{\mathrm{LR\text{-}NON}}$. The average number concentration of newly formed particles for high- and low-radiation days were calculated as

$$\overline{N}_{\mathrm{NPF\text{-}HR}} = \frac{\int_0^{24} \left(\tilde{N}_{\mathrm{HR\text{-}NPF}} - \tilde{N}_{\mathrm{HR\text{-}NON}}\right) \times \mathrm{d}t}{24} \quad \text{and} \quad (8)$$

$$\overline{N}_{\mathrm{NPF\text{-}LR}} = \frac{\int_0^{24} \left(\tilde{N}_{\mathrm{LR\text{-}NPF}} - \tilde{N}_{\mathrm{LR\text{-}NON}}\right) \times \mathrm{d}t}{24}, \quad (9)$$

respectively. Accordingly, the overall contribution of NPF events to UFP concentration could be calculated as

$$\overline{N}_{\mathrm{NPF}} = \frac{\overline{N}_{\mathrm{NPF\text{-}HR}} \times n_{\mathrm{NPF\text{-}HR}} + \overline{N}_{\mathrm{NPF\text{-}LR}} \times n_{\mathrm{NPF\text{-}LR}}}{n_{\mathrm{NPF\text{-}HR}} + n_{\mathrm{NPF\text{-}LR}} + n_{\mathrm{NON\text{-}HR}} + n_{\mathrm{NON\text{-}LR}}}, \quad (10)$$

where $n_{\mathrm{NPF\text{-}HR}}$ ($n_{\mathrm{NPF\text{-}LR}}$) and $n_{\mathrm{NON\text{-}HR}}$ ($n_{\mathrm{NON\text{-}LR}}$) are the number of high-radiation (low-radiation) days with and without NPF events, respectively.

2.3.5 Enhancement in CCN number concentration

The NPF-initiated enhancements in CCN number concentration (N_{CCN}), denoted $E_{N_{\mathrm{ccn}}}$, were quantified using the method proposed by Ren et al. (2021) and Kalkavouras et al. (2019). This approach compares the N_{CCN} after and prior to the NPF event:

$$E_{N\mathrm{ccn}} = N_{\mathrm{CCN\_after}}/N_{\mathrm{CCN\_prior}}, \quad (11)$$

where $N_{\mathrm{CCN\_prior}}$ is the 2 h average of N_{CCN} before the start of NPF and $N_{\mathrm{CCN\_after}}$ is determined as the average N_{CCN} during the period that NPF contributes to N_{CCN}. As a simplified estimate, N_{CCN} was calculated as the integral PNC with a particle size larger than the pre-defined critical diameter (D_{C}). Referring to a previous study by Wu et al. (2015), D_{C} values of 50, 70, and 180 nm were applied for 0.6 %, 0.4 %, and 0.1 % supersaturation, respectively. The start and end times of the period when NPF impacts N_{CCN} were determined by evaluating the variability in normalized time series of N_{CCN} for each prescribed supersaturation. Details regarding the approach can be found in Kalkavouras et al. (2019) and Ren et al. (2021). It should be noted that this method is based on the assumption that the background concentration of CCN stays constant during NPF, ignoring the influence of other sources and sinks of aerosol particles; therefore it can only give a rough estimate of the impact of NPF on N_{CCN}.

2.3.6 Enhancement in the extinction coefficient

The influence of NPF on radiative forcing was evaluated based on the measured PNSD and eBC mass concentration using Mie theory (Mie, 1908). Assuming that black carbon (BC) is internally mixed and its volume fraction is independent of particle size, a uniform volume fraction of BC ($\mathrm{VF_{BC}}$) for different particle sizes is defined as

$$\mathrm{VF_{BC}} = \overline{V}_\mathrm{BC}/\overline{\mathrm{PVC}}, \tag{12}$$

where $\overline{V}_\mathrm{BC}$, the mean volume concentration of BC particles, is obtained by the mean eBC mass concentration during the observation period divided by the density of BC ($1.5\,\mathrm{g\,cm^{-3}}$). $\overline{\mathrm{PVC}}$ is the average integral particle volume concentration (PVC) calculated from the measured PNSD.

Accordingly, the refractive index is derived as a volume-weighted average of BC and the non-absorbing component:

$$\overline{m} = \mathrm{VF_{BC}} \times \overline{m}_\mathrm{BC} + (1 - \mathrm{VF_{BC}}) \times \overline{m}_\mathrm{non\text{-}abs}, \tag{13}$$

where the refractive index for BC is set as $\overline{m}_\mathrm{BC} = 1.96 - 0.66i$ (Seinfeld et al., 1998) and the non-absorbing component is set as $\overline{m}_\mathrm{non\text{-}abs} = 1.53 - 10^{-7}i$ (Wex et al., 2002).

The dimensionless extinction efficiency Q_ext can be obtained using Mie theory (Mie, 1908), and the extinction coefficient σ_ext can be calculated accordingly as

$$\sigma_\mathrm{ext} = \int_{D_P} Q_\mathrm{ext} \times (\frac{\pi}{4} D_P^2) \times \mathrm{PNSD} \times \mathrm{dlog} D_P. \tag{14}$$

Similarly to the CCN enhancement estimation in Sect. 2.3.5, the NPF-initiated enhancement of the aerosol extinction coefficient (E_ext) was quantified as

$$E_\mathrm{ext} = \sigma_\mathrm{ext\_after}/\sigma_\mathrm{ext\_prior}, \tag{15}$$

where $\sigma_\mathrm{ext\_prior}$ is the 2 h average of σ_ext before the NPF start and $\sigma_\mathrm{ext\_after}$ is determined as the average σ_ext during the period with NPF influence as described in Sect. 2.3.5.

3 Results I: basic features of NPF

3.1 NPF occurrence frequency

Table 2 presents the occurrence frequencies of NPF events observed at each site from 2009–2013, and a comparison of NPF occurrence frequency between GUAN sites and other European studies will be discussed in this section.

It should be noted that there are data missing for 1 to 3 years in four of the nine GUAN sites (Fig. S1). A question raised is whether the missing data may cause an issue of data representativeness. For UB sites, LTR and LWE had missing data in 2013 and 2009–2010, respectively. The sites LTR and LWE are both located in the city of Leipzig and are only 10 km apart. As can be seen from Fig. S2, the NPF occurrence frequencies at the two sites were quite close during the overlapping period from June 2011–December 2012.

Meanwhile, no significant inter-annual variation was found in the 4-year data of LTR and 3-year data of LWE. For RB sites, the observation at NEU was unavailable from 2019–2010. Both NEU and WAL can represent the regional background air in the northern German lowlands, and no significant inter-annual variation in NPF occurrence frequency was found at WAL. Hence, we assume that the influence of the inter-annual changes on the characteristics of NPF in LTR, LWE, and NEU was limited and that the available dataset of these three sites can represent the overall characteristics of NPF for the 5-year period. Among the three mountainous sites, ZSF had the least valid data, with only 2012 and 2013 available. The regional air mass occurrence frequency at ZSF increased slightly with a rate of $0.96\,\%\,\mathrm{yr^{-1}}$ from 2009–2013 (Sun et al., 2021), resulting in more frequent vertical transport of precursor gases to high altitudes. The occurrence of NPF depends on several local conditions such as precursor concentration, CS, temperature, and solar radiation. However, the inter-annual variation in regional air mass occurrence frequency may imply that the characteristics of NPF at ZSF for 2012 and 2013 might be slightly biased by those for the whole period of 2009–2013.

The NPF occurrence frequencies at the sites in the same category were found to be similar. The RB sites had the highest NPF occurrence frequency, with an average of about 19 %, followed by the UB sites with an average of about 15 %. NPF events were observed on about 7 % of days at LMT sites and only about 3 % of days at the HA site ZSF. A previous study by Nieminen et al. (2018) found similar annual and seasonal occurrence frequencies for MEL and HPB. It is interesting that a lower occurrence frequency of NPF is found at ZSF compared to the two LMT sites. The atmosphere in high-altitude areas can be influenced by both PBL and FT (Sun et al., 2021; Herrmann et al., 2015; Rose et al., 2017). Additionally, NPF has been found to be strongly associated with the air parcel vertically transported from lower altitudes (Bianchi et al., 2016; Shen et al., 2016; Tröstl et al., 2016). The influence of vertical transport of PBL air mass is much weaker at ZSF than lower altitudes, leading to a lower CS and concentrations of precursors (Collaud-Cohen et al., 2018). As reported in Flentje et al. (2010), the median SO_2 mass concentration during the years 2000–2007 at ZSF was about $0.18\,\mathrm{\mu g\,m^{-3}}$, which was lower than the one at HPB ($0.31\,\mathrm{\mu g\,m^{-3}}$). Therefore, though the low temperature and CS at ZSF favor NPF, the extremely low concentration of precursors at ZSF inhibits the occurrence of NPF, which is likely to be one of the reasons for the lower NPF occurrence frequency at ZSF.

Figure 2 compares the overall NPF occurrence frequencies at the GUAN sites with those of other sites in Europe (Baalbaki et al., 2021; Boulon et al., 2011; Bousiotis et al., 2019, 2021b; Brines et al., 2015; Dameto De España et al., 2017; Herrmann et al., 2015; Hofman et al., 2016; Joutsensaari et al., 2018; Lee et al., 2020; Manninen et al., 2010; Németh et al., 2018; Nieminen et al., 2014; Plauskaite et al., 2010;

Table 2. Annual occurrence frequency, average growth, and formation rates of NPF events at each observation site.

Site category	Site name	NPF occurrence frequency	Undefined event occurrence frequency	GR_{10-25} $(nm\,h^{-1})$	J_{10-25} $(cm^{-3}\,s^{-1})$
Urban background (UB)	LTR	16.8 %	15.7 %	4.4	2.8
	LWE	15.5 %	14.5 %	4.4	2.9
	BOS	12.6 %	14.6 %	4.1	1.9
Regional background (RB)	MEL	19.6 %	16.9 %	4.7	2.0
	NEU	18.3 %	20.6 %	4.3	1.2
	WAL	19.0 %	19.9 %	4.1	1.6
Low-mountain-range (LMT)	HPB	6.8 %	15.4 %	3.7	0.6
	SCH	7.8 %	17.3 %	3.8	0.5
High Alpine (HA)	ZSF	3.4 %	14.3 %	3.8	0.4

Salma and Németh, 2019; Sellegri et al., 2019; Smejkalova et al., 2021; Vaananen et al., 2013; Vana et al., 2016). For detailed information on the locations of those observation sites and study periods, please refer to Table S1 in the Supplement.

The NPF occurrence frequencies at the three UB sites in GUAN were found to be similar to those of other UB sites in central Europe, such as in Amsterdam (AMS), Budapest (BDP), and Vienna (VIE). The annual NPF occurrence frequencies at the three RB sites in GUAN were in the medium range of all RB sites, as illustrated in Fig. 2. The highest NPF occurrence frequency was observed at the Agia Marina Xyliatou (AMX) site in Cyprus, with an occurrence frequency of 57 % and 8 % for NPF and undefined events, respectively. Generally, the site-to-site differences in NPF occurrence frequency are the result of many factors such as location, meteorological conditions, and anthropogenic and biogenic emissions in the vicinity of the observation sites (Nieminen et al., 2018). For example, a higher NPF occurrence frequency was observed at the AMX and Cabauw (CBW) sites than MEL. One possible explanation is that both AMX and CBW are more affected by marine air masses (Manninen et al., 2010; Németh et al., 2018), while MEL is affected more by biogenic emissions from the surrounding forested areas (Bousiotis et al., 2021). When comparing the NPF occurrence frequency among different studies, the regional representativeness of an individual observation site should be fully considered. Additionally, care should be taken when comparing NPF features, since the NPF events were visually classified. The subjective preference in the classification process may introduce bias into NPF occurrence frequencies. For instance, the occurrence frequencies of NPF events at mountainous sites in GUAN were much lower than those of other mountainous sites. In particular, the occurrence frequency of NPF was only 3.4 % at ZSF, while it was 14.5 % for another HA site, Jungfraujoch (JFJ), in Herrmann et al. (2015). In the visual classification process by Dal Maso et al. (2005), the potential NPF days can be classified as NPF events or undefined events. As stated by Herrmann
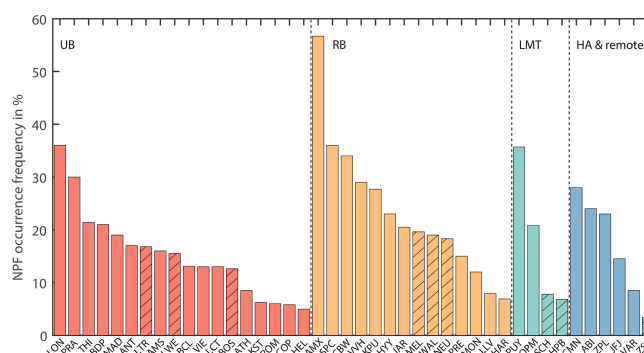
Figure 2. Annual occurrence frequency of NPF events in the present study and other studies in Europe. The hatched pattern denotes the results for the GUAN sites in this study.

et al. (2015), the occurrence frequencies of NPF events and undefined events are 14.5 % and 5.4 %, respectively, for JFJ. The corresponding values are 3.3 % and 15.2 %, respectively, for ZSF. This large discrepancy in the NPF occurrence frequency between these two sites may result from subjective decisions when classifying the dataset into NPF and undefined events during the visual classification process.

Figure 3 shows the monthly NPF occurrence frequencies of the nine GUAN sites, and a comparison of the seasonal occurrence frequency of NPF between the nine GUAN sites and other European sites is illustrated in Fig. S2 in the Supplement. For most sites, the highest occurrence of NPF was found during spring and summer, while the lowest was in winter, which is consistent with observations in previous studies (e.g., Nieminen et al., 2018; Salma and Németh, 2019; Boulon et al., 2011). Such a seasonal pattern is highly related to the seasonal variations in solar radiation and biogenic emissions (Manninen et al., 2010). The seasonal variation in NPF occurrence frequency also differed among site categories. In early autumn (September and October), NPF events occurred more frequently in RB sites than in UB sites, likely due to the high emission of biogenic VOCs in rural

areas in autumn (Salma et al., 2016). Furthermore, the seasonal pattern of NPF events varied among mountainous sites, as shown in Fig. 3. This variability may be a result of the upslope valley winds, which can have a different impact on different sites and seasons depending on the altitude and topography of the site (Nieminen et al., 2018).

3.2 Growth and formation rates

Figure 4 shows the basic statistics of annual GR_{10-25}, J_{10-25}, and CS at the nine GUAN sites. The growth and formation rate were only evaluated for type I events in this study, and CS was estimated for all NPF event days. As listed in Table 2, the annual mean GR_{10-25} for particle sizes of 10–25 nm varied from 3.7 to 4.7 nm h^{-1}, with surprisingly minor differences between the sites. Previous studies also found that GR varies little among different sites and exhibits only very weak dependency on the low-volatility vapor concentration, particularly in a fixed site (Kulmala et al., 2022a, 2023). However, the site-to-site comparison of J_{10-25} implied that stronger anthropogenic influences could lead to a higher J_{10-25}, which is consistent with previous studies (e.g., Bousiotis et al., 2021b; Nieminen et al., 2018; Sebastian et al., 2022). The site-to-site difference in anthropogenic influences can be clearly seen from the mean PNSD on non-event days, as shown in Figs. S5 and S6 in the Supplement. Similarly, the CS values were generally higher in the area with stronger anthropogenic emissions and the lowest at the HA site ZSF. CS and J_{10-25} at BOS were lower than the other two UB sites in Leipzig, suggesting relatively few anthropogenic emissions at BOS compared to LTR and LWE. Additionally, it should be noted that both LTR and LWE are located in the urban background of Leipzig. The occurrence frequencies and start times of NPF (Sect. 3.3) were similar at the two sites, while GR_{10-25} and J_{10-25} were not. One possible explanation for such differences in GR_{10-25} and J_{10-25} may be the different surroundings of the two sites. LTR is located on the top of a three-floor building about 100 m from a main road and therefore is more influenced by traffic emissions. The LWE is located in a park 30 m from a minor road, so the impact of fresh traffic emissions is negligible (Birmili et al., 2016). As shown in Fig. S6a3 and b3, the PNC of particles with diameters lower than 50 nm at LTR was higher than that at LWE. One of our previous studies showed that the PNCs in the traffic-related size ranges N_{10-30} and N_{30-200} were 10 % and 17 % higher, respectively, at LTR and LWE (Sun et al., 2019), indicating higher gaseous precursor concentrations and thus a stronger anthropogenic influence at LTR.

Figure 5 displays the annual GR measured at GUAN sites and other European sites (Boulon et al., 2011; Bousiotis et al., 2019, 2021b; Herrmann et al., 2015; Kalkavouras et al., 2020; Lee et al., 2020; Manninen et al., 2010; Nieminen et al., 2014, 2018; Salma et al., 2016; Tröstl et al., 2015; Vaananen et al., 2013; Vana et al., 2016). For the GR values and the

corresponding size range reported in those studies, please refer to Table S2 in the Supplement. GR_{10-25} for GUAN sites falls within the range of values reported in previous European studies. Caution should be taken because the differences in observation periods and size ranges of GR may influence the comparison among sites. In UB sites, the highest GR was reported at Budapest (BUD), with a size range of 6–50 nm. LWE, Kensington (KST), and LTR showed a similar GR level, but the size range of GR at KST was 16.6–50 nm. The lowest GR values in UB sites were observed at Copenhagen (COP) and Helsinki (HEL), with evaluated size ranges of 5.8–30 and 3.4–30 nm, respectively. Regarding RB sites, GR at the CBW site was about 6.6 nm h^{-1}, which was much higher than at other RB sites. This high GR at CBW may result from the short observation period in this study, from 1 April 2008 to 31 March 2009 (Manninen et al., 2010). Meanwhile, another study has reported the seasonal variation in GR at CBW between 10 and 25 nm as well (Nieminen et al., 2018). The seasonal GR_{10-25} ranged from 2.9 to 4.9 nm h^{-1}, which was similar to GR_{10-25} at the RB sites of GUAN. For LMT sites, GR_{10-25} values at SCH and HPB were lower than the GR_{7-20} values at another two LMT sites, Puy de Dôme (PUY) and Opme (OPM), located in central France. Nieminen et al. (2018) also found that GR_{10-25} at PUY was significantly higher than those values at other LMT sites, possibly related to the vertical transport of particles within the boundary layer. For high-altitude and remote sites, the GR_{10-25} of ZSF was comparable to those of other sites.

Figures 6 and 7 present the seasonal GR_{10-25} and J_{10-25} at GUAN sites in this study. Since GR_{10-25} and J_{10-25} were only evaluated for type I events, there were NPF events observed in wintertime but no GR_{10-25} and J_{10-25} evaluated at some sites, for example at NEU. The highest GR_{10-25} was observed in summer for most sites, while the lowest was observed in winter. Many previous studies have also reported such seasonal pattern, especially in regional background areas, which have been attributed to enhanced biogenic aerosol precursors and stronger solar radiation during summer (Nieminen et al., 2014; Kerminen et al., 2018; Asmi et al., 2011). Both LTR and LWE are located in the city of Leipzig, and the different seasonal variations in GR_{10-25} may be due to the different degrees of urban emissions at these two sites, as discussed in Sect. 3.1. The seasonal variations in J_{10-25} were similar to those in GR_{10-25} in UB and RB sites, with the universal maximum observed in summer. However, a different seasonal pattern for the three mountainous sites was observed, with the maximum J_{10-25} being reached in spring. This seasonal behavior was observed for the HPB site in a previous study by Nieminen et al. (2018) as well. Another exception to the seasonal pattern of GR_{10-25} and J_{10-25} was NEU, which had clearly lower GR_{10-25} and J_{10-25} values in summer compared to spring; these values may have been underestimated due to missing data.
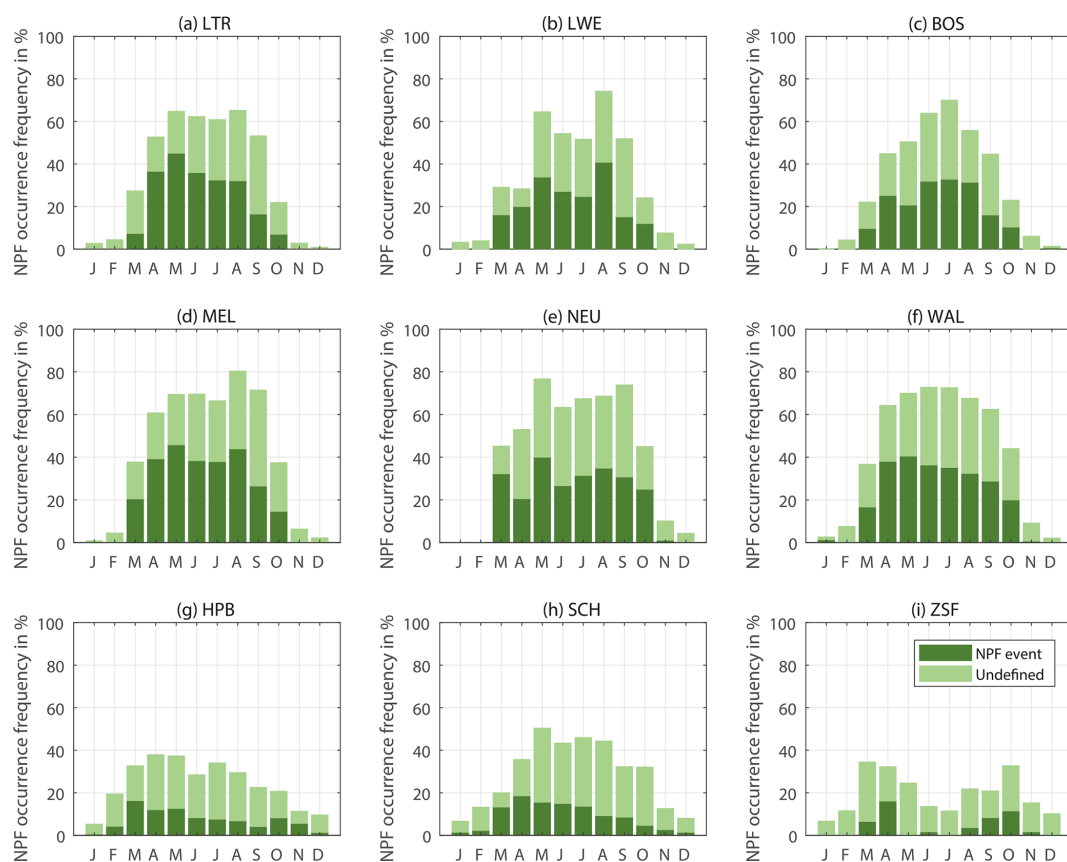
Figure 3. Monthly occurrence frequencies of NPF events for the nine GUAN sites. The dark-green bar denotes the occurrence frequencies of the NPF events (type I and II), and the light-green bar denotes those of undefined events.

3.3 Start time of NPF events

Figure 8 shows the estimated start time of type I events as a function of the day of year. The start time was initially estimated based on local time (UTC+1) and further converted to solar time according to the longitude of the sites. The PNSD observations in our dataset were initiated from particle sizes from 5 or 10 nm at different sites (Table 1). However, the start time at 10 nm ($t_{10\,nm}$) was not able to describe the actual occurrence time of nucleation. Therefore, $t_{10\,nm}$ has been converted to the critical nucleation diameter of 2 nm ($t_{2\,nm}$) using the GR_{10-25} values by $t_{2\,nm} = t_{10\,nm} - \frac{(10-2)}{GR_{10-25}}$.

Typically, most NPF events started between 07:30 and 09:00 solar time at all GUAN sites. Seasonal variations in the start time were evident, with earlier start times in summer due to earlier sunrise times. It is noteworthy that the differences in the start time of NPF events exist between sites, as shown in Figs. 8 and S7 in the Supplement. The three mountainous sites (HPB, SCH, and ZSF) had the latest start time of around 09:00. Two UB sites, LTR and LWE, had the earliest start time of around 07:30. The start time at BOS and the three RB sites (MEL, WAL, and NEU) was around 08:30. Since the use of solar time has already eliminated the bias of local time relative to site longitude, the difference in start time

among sites mainly stems from the different diurnal variations in precursor concentration and CS. Figure S8 shows the mean diurnal cycle of CS on NPF days for all nine GUAN sites. CS at UB sites increases rapidly during morning rush hour due to the strong traffic emissions in urban areas, also implying an increase in precursor concentration. The ratio of sources to sinks may be changed during this time period and further leads to an earlier NPF start time in urban areas than at RB sites. In the mountain area, CS starts to increase at about 08:00 and reaches its daily maximum in the late afternoon, meaning that it may take some time for the development of the boundary layer and transport of the precursors upward after sunrise, resulting in a late NPF start time.

4 Results II: environmental and climate-relevant effects

4.1 Contribution of NPF to ultrafine particles

NPF events are believed to be a significant source of UFPs. In this section, the contribution of NPF to UFP number concentration was qualitatively and quantitatively evaluated using two approaches by Salma et al. (2017) and Ma and Birmili (2015).
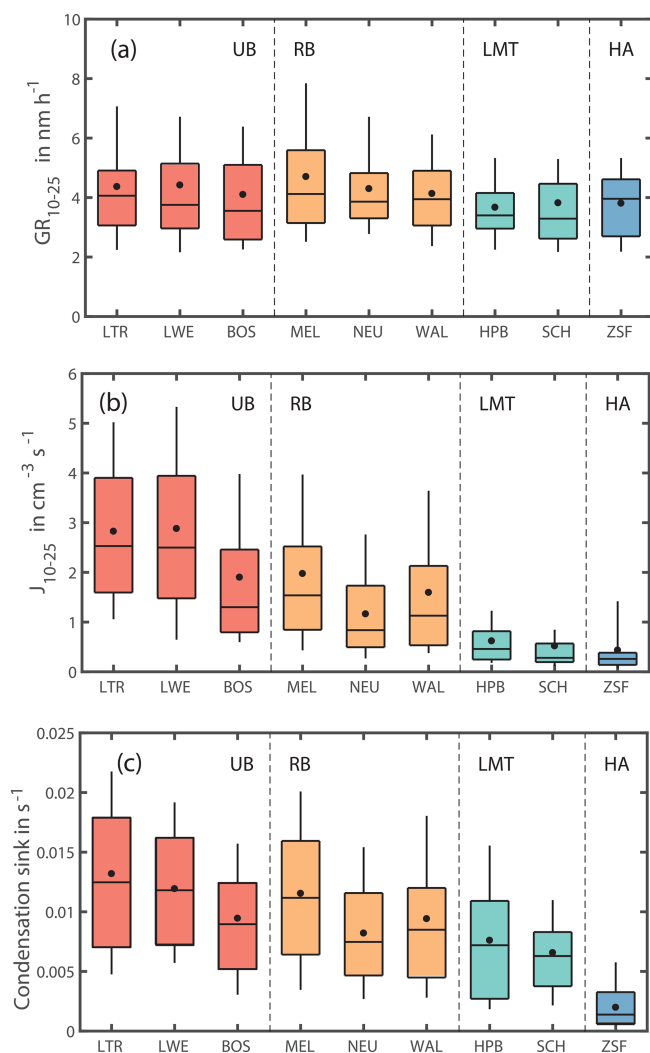
Figure 4. Basic statistics of GR_{10-25}, J_{10-25}, and the condensation sink measured at the GUAN sites. Dots denote the mean values, and the boxes and whiskers denote the 10th, 25th, 50th, 75th, and 90th percentiles.
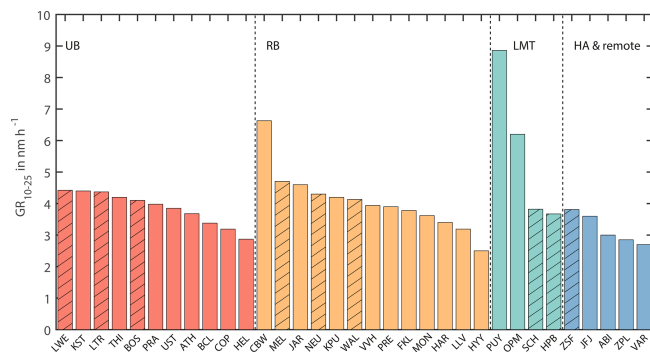
Figure 5. Average GR_{10-25} in the present study and other studies in Europe. The hatched pattern denotes the results for the GUAN sites in this study.

4.1.1 Nucleation strength factor

The nucleation strength factor (NSF) is a simple metric to qualitatively estimate the relative concentration increment of UFP number concentration on NPF days. As stated in Salma et al. (2017), an NSF of 1 indicates that the relative contribution of NPF events to UFPs is negligible, while a value > 2 suggests that NPF can be considered a dominant source of UFPs at the site on NPF days. Figure 9 compares the annual median NSF among the nine GUAN sites and those values reported in an earlier study by Bousiotis et al. (2021b). The NSF was around 2 for all RB and mountainous sites, implying that NPF events were the dominant source on NPF days in those environments. The NSF was much lower at UB sites, typically ranging between 1 and 2. Ma and Birmili (2015) reported that aged traffic and other urban sources contributed around 40 % and 30 % to N_{5-100} and N_{20-100} at LTR, respectively. Higher anthropogenic emissions result in a higher UFP number concentration and thus a lower NSF in urban areas. Such high contributions from anthropogenic sources lead to an increased CS, causing more new particles to be scavenged by the more polluted atmosphere and resulting in a lower NSF in urban areas. In addition, the mean PNSD on NPF and non-event days for each GUAN site in Fig. S6 can clearly depict this site-to-site difference in the NSF. The anthropogenic influence on UFPs gradually decreased from UB to HA sites, leading to a clearer background atmosphere for RB and mountainous areas. Hence, the contribution of NPF to UFPs was more pronounced in these site categories.

4.1.2 Quantitative contribution to UFPs

Another approach was further implemented to derive a quantitative average contribution of NPF to UFPs. The diurnal cycle of the UFP increment on NPF days with high and low solar radiation was estimated, as described in Ma and Birmili (2015). In our study, the UFPs were assumed to originated from "NPF" and "other sources", in which the latter encompassed all non-NPF sources such as fresh local traffic, aged traffic, other urban sources, and regional backgrounds.

Figure 10 displays the absolute and relative contributions of NPF to UFPs (N_{10-100}) at seven GUAN sites, and Fig. 11 shows the monthly relative contributions. The analysis did not include BOS and ZSF due to the absence of solar radiation data at these sites. As seen in the two figures, the highest contribution of NPF to UFPs was found for the RB sites, with contributions of around 25 % at MEL and NEU and 15 % at WAL. For the two UB sites, LTR and LWE, the contributions of NPF were lower, accounting for 11 % and 15 %, respectively, of N_{10-100}. As discussed in Ma and Birmili (2015), regional background aerosols contribute to UFPs equally for urban background (LTR) and nearby regional background (MEL) sites. However, some urban sources such as aged traffic also contribute to UFPs at UB sites, resulting in a lower relative contribution of NPF to UFPs at these sites. Due to the
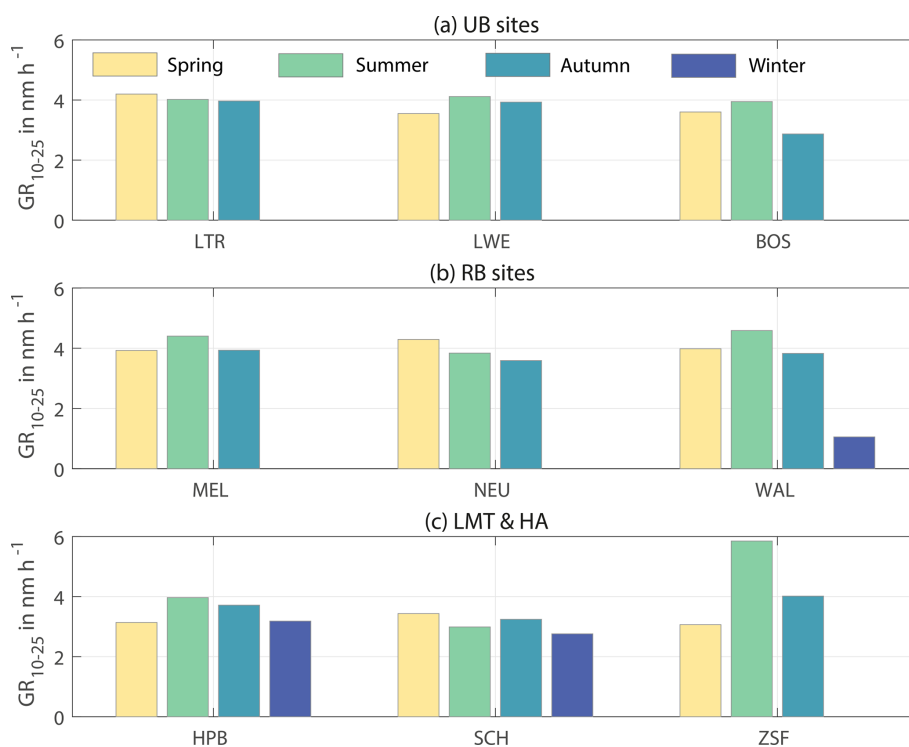
Figure 6. Seasonal mean GR_{10-25} of NPF events for the nine GUAN sites.

low occurrence and low nucleation rate of NPF at the mountainous sites (Table 2), the contribution of NPF to UFPs was the lowest at HPB and SCH, accounting for 5 % and 9 % of N_{10-100}, respectively.

Pronounced seasonal variations in the relative contributions of NPF to UFPs were found for all seven GUAN sites (Fig. 11), with a higher contribution from May to August and almost no contribution in winter. The contribution of NPF to UFPs is determined by many factors such as the frequency, nucleation rate, and growth rate of NPF, as well as the concentration of particles from other sources. The contribution of NPF is proportional to the frequency of NPF if other factors remain unchanged. Therefore, the seasonal patterns of the relative contributions of NPF were very similar to the seasonal variation in NPF occurrence frequency for each site (Fig. 3). The highest relative contributions of NPF to UFPs were observed during summer (from May to August), with ranges of 30 %–48 % and 41 %–56 % at UB and RB sites, respectively. However, the seasonal distributions of NPF contribution observed at the mountainous sites were similar to those of NPF occurrence frequency in Fig. 3, peaking in spring from March to May with values from 14 %–23 %.

4.2 Contribution of NPF to cloud nuclei condensation (CCN)

To evaluate the potential contribution of NPF to CCN, the relative enhancement of CCN number concentration (N_{CCN}

enhancement, denoted $E_{N_{ccn}}$), which is the ratio of N_{CCN} after the NPF event to that prior to NPF event, has been estimated following an approach proposed by previous studies (Kalkavouras et al., 2019; Ren et al., 2021). It should be noted that during an NPF event, both the newly formed particles and the pre-existing particles can grow to a CCN-relevant size. The pre-existing particles have larger diameters and may reach a CCN-relevant size faster than newly formed particles and therefore may even have a larger contribution to CCN number concentration. Kalkavouras et al. (2019) stated that the pre-existing particles may induce a bias in the estimated CCN enhancement of up to 50 %. It is difficult to decompose the contributions of the two parts, so the $E_{N_{ccn}}$ estimated in this study was an integrated CCN number concentration enhancement contributed by both parts during NPF events.

Table 3 summarizes $E_{N_{ccn}}$ on NPF days in our study and other studies previously conducted in Europe. Our dataset shows a pattern similar to the results from previous studies (Rejano et al., 2021; Kerminen et al., 2012; Dameto et al., 2017; etc.), with higher $E_{N_{ccn}}$ associated with a weaker influence of anthropogenic emissions. However, exceptions were found for the BOS and NEU sites, where $E_{N_{ccn}}$ was much higher than the one at the other sites in the same site categories. The seasonal distribution of $E_{N_{ccn}}$ (Fig. S9 in the Supplement) at BOS indicated that the elevated N_{CCN} enhancement may be due to a significantly higher $E_{N_{ccn}}$ in autumn, and the higher $E_{N_{ccn}}$ at NEU may be attributed to seasonal
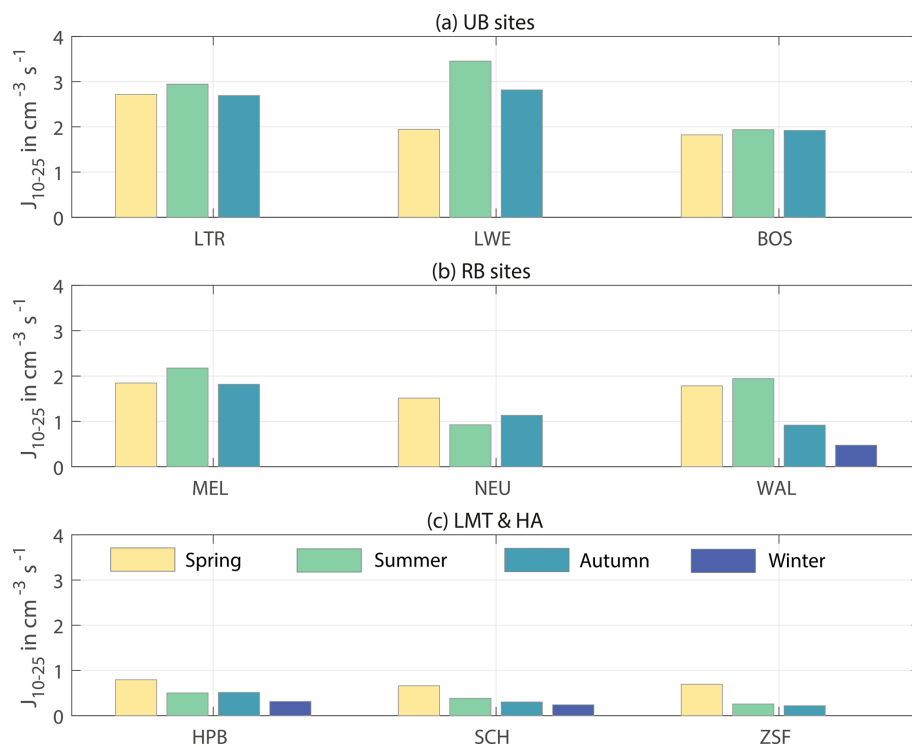
Figure 7. Seasonal mean J_{10-25} for NPF events at the nine GUAN sites.
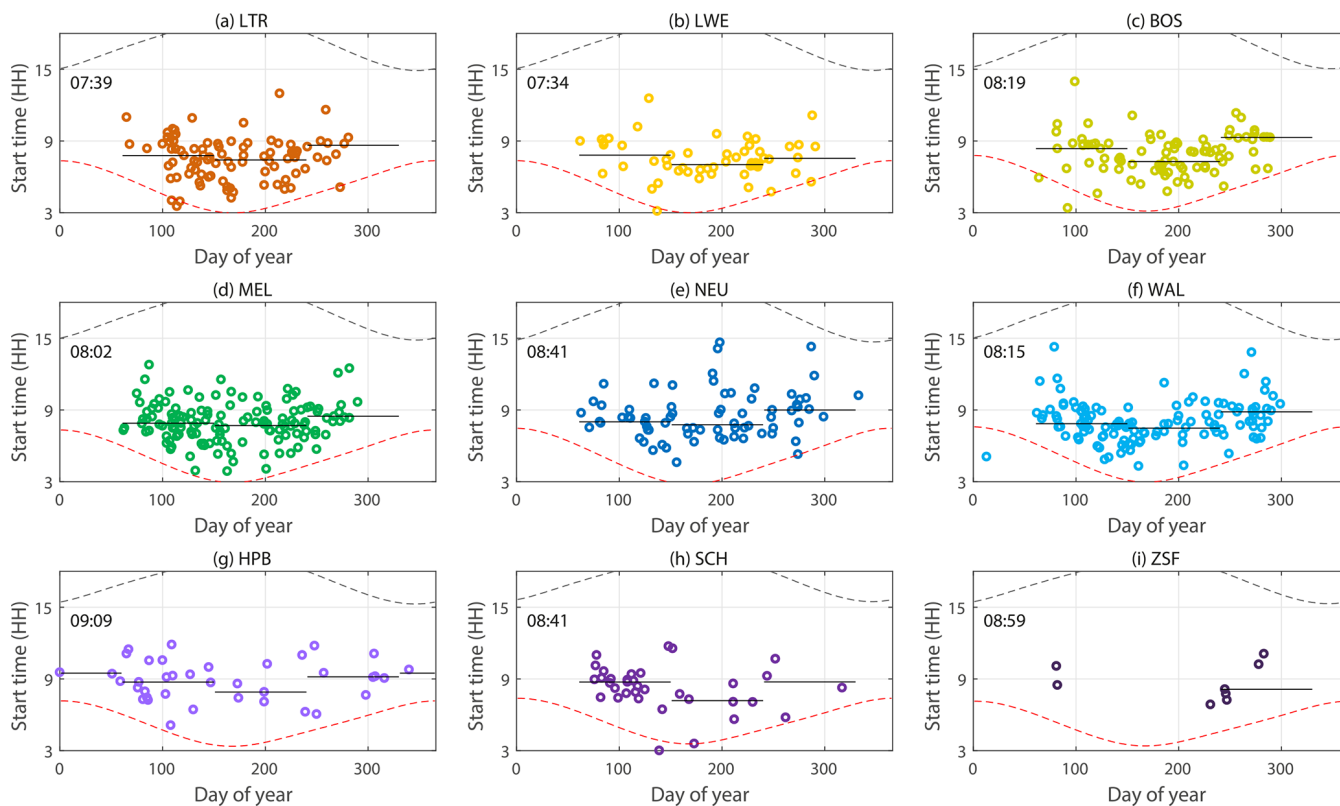
Figure 8. Scatterplot of the NPF start time (solar time) on different days of year. Solid black lines denote the mean seasonal start time, and the dashed red and black lines indicate the sunrise and sunset time, respectively.
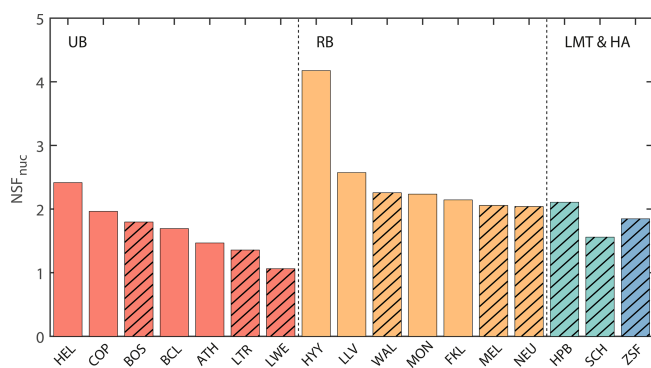
Figure 9. The median NSF in the present study and other studies in Europe. The hatched pattern denotes the results for the GUAN sites in this study.

bias in data availability. The highest $E_{N_{ccn}}$ was observed in the three mountainous sites due to the low background PNC in those areas (Kerminen et al., 2012).

When comparing our results with other studies in Table 3, it is important to proceed with caution because the significant variation in $E_{N_{ccn}}$ may result from different observation periods, assumed supersaturation levels, critical diameters D_C, and N_{CCN} estimation methods. However, some consistencies can still be found. For example, $E_{N_{ccn}}$ at the UB site of Vienna was similar to those at the UB sites in GUAN, and $E_{N_{ccn}}$ values at RB sites in Finland and Sweden are comparable to those for our sites. Other studies have reported $E_{N_{ccn}}$ for the MEL and HPB sites as well. The results from the present study are consistent with those from a long-term observation study by Ren et al. (2021) but lower than another short-term NPF case study by Wu et al. (2015).

The observed $E_{N_{ccn}}$ in this study revealed a clear relationship between $E_{N_{ccn}}$ and the degree of anthropogenic emission influence in diverse environments. However, it is important to bear in mind that the estimation of $E_{N_{ccn}}$ is based on a constant D_C and may result in overestimation, as stated by Wu et al. (2015). Besides, the $E_{N_{ccn}}$ estimation accounted only for NPF days and not for the entire observation period. That is, the NPF occurrence frequency was not taken into consideration. We need to be careful when interpreting the $E_{N_{ccn}}$ values, especially for those high $E_{N_{ccn}}$ values in clean areas in Table 3. Accounting for the high $E_{N_{ccn}}$ but low NPF occurrence frequency in those clean areas, it cannot be concluded that NPF events have a significant impact on the overall CCN budget at those sites.

4.3 Impact of NPF on the aerosol extinction coefficient

The growth of newly formed particles into large sizes during NPF may subsequently affect bulk aerosol optical properties and further impact the regional aerosol radiative forcing and climate. However, the impact of NPF on aerosol optical properties has been discussed in only a few studies. For instance, Shen et al. (2011) analyzed the enhancement of the aerosol extinction coefficient during the evolution of an NPF event in an RB site in China. To investigate the contribution of NPF to the aerosol extinction coefficient for diverse environments, the ratio of the averaged aerosol extinction coefficient at 550 nm ($\sigma_{ext,\,550\,nm}$) after each NPF event to that before each NPF event was evaluated in this section, namely $\sigma_{ext,\,550\,nm}$ enhancement. The start and end points for each NPF event were adopted from those for N_{CCN} enhancement evaluation, described in Sect. 4.2. The $\sigma_{ext,\,550\,nm}$ enhancement and the corresponding statistical significance are listed in Table 4. Statistically insignificant contributions were found for the other sites, especially for polluted urban sites. However, NPF events occurring in areas with low background PNC and low anthropogenic emissions, such as the RB site NEU and the three mountainous sites, can significantly enhance $\sigma_{ext,\,550\,nm}$ on NPF event days. These findings underscore the importance of considering the impact of NPF on optical properties when assessing aerosol radiative forcing, especially in remote regions. Besides, similarly to the $E_{N_{ccn}}$ estimation, the enhancement of $\sigma_{ext,\,550\,nm}$ was only for NPF days. The results in Table 4 cannot represent the NPF enhancement of $\sigma_{ext,\,550\,nm}$ over the whole study period.

When discussing the aforementioned environmental and climate-relevant effects of NPF, it is important to bear in mind that the contribution obtained is likely to be underestimated. One reason for this is the potential of missing cases where NPF is relatively weak or interrupted by changed air masses during measurements. These occurrences, known as "quiet NPF" phenomena, have been found to contribute to the secondary particles in the atmosphere (Kulmala et al., 2022b). Another reason is that it is difficult to follow the growth of newly formed particles for longer than a few hours (certainly less than a day) in a single-site measurement, yet the growing particles remain in the ultrafine range for 1–3 d (the time it takes for them to reach the CCN size). As a result of these considerations, a substantial portion of the UFPs in the troposphere classified as "background" or "other sources" are actually formed by NPF, either via unclear or weak events or 1–3 d upwind of the measurement site, leading to an underestimation of the relevance effects discussed above.

5   Conclusions

Based on a 5-year dataset of the German Ultrafine Aerosol Network (GUAN), this study investigated the characteristics of NPF for various environments from urban background

Table 3. Comparison of the enhancement of CCN by NPF (N_{CCN} enhancement, $E_{N_{ccn}}$) from multiple European studies.

Site	Site category	Time period	CCN method	Critical diameter (nm)	Supersaturation (ss) (%)	$E_{N_{ccn}}$	Reference
LTR, Germany	UB	2009–2013	Calculated	190, 80, 60	0.1, 0.4, 0.6	1.0, 1.3, 1.2	This study
LWE, Germany	UB	2011–2013	Calculated	190, 80, 60	0.1, 0.4, 0.6	1.0, 1.1, 1.2	
BOS, Germany	UB	2009–2013	Calculated	190, 80, 60	0.1, 0.4, 0.6	1.2, 1.6, 1.6	
MEL, Germany	RB	2009–2013	Calculated	190, 80, 60	0.1, 0.4, 0.6	1.1, 1.2, 1.3	
NEU, Germany	RB	2011–2013	Calculated	190, 80, 60	0.1, 0.4, 0.6	1.3, 1.5, 1.5	
WAL, Germany	RB	2009–2013	Calculated	190, 80, 60	0.1, 0.4, 0.6	1.0, 1.2, 1.3	
HPB, Germany	LMT	2009–2013	Calculated	190, 80, 60	0.1, 0.4, 0.6	1.6, 1.7, 1.8	
SCH, Germany	LMT	2009–2013	Calculated	190, 80, 60	0.1, 0.4, 0.6	1.5, 1.8, 1.9	
ZSF, Germany	HA	2012–2013	Calculated	190, 80, 60	0.1, 0.4, 0.6	1.9, 1.8, 1.9	
Vienna, Austria	UB	2014–2015	Measured	57	0.5	1.4	Dameto et al. (2017)
University of Crete, Greece	Coastal	2008–2015	Measured	162, 67, 54, 46, 43, 35	0.1, 0.4, 0.5, 0.7, 0.7, 1.0	1.3–1.8	Kalkavouras et al. (2019)
Sierra Nevada National Park, Spain	High altitude	2018–2019	Measured	66	0.5	1.8	Rejano et al. (2021)
Hyytiälä, Finland	RB	2008–2009	Measured		0.1, 0.2, 0.4, 0.8, 1.0	2.1, 2.1, 1.7, 1.8, 1.7	Sihto et al. (2011)
MEL, Germany	RB	May–June 2008	Calculated	Varied	0.1, 0.4, 0.6	1.6, 1.7, 1.7	Wu et al. (2015)
MEL, Germany	RB	May 2017	Calculated		0.2, 0.4, 0.8	1.0, 1.3, 1.7	Ren et al. (2021)
HPB, Germany	LMT	October 2015	Calculated		0.2, 0.4, 0.8	0.9, 1.1, 1.5	
Vavihill, Sweden	RB	October 2009	Calculated		0.2, 0.4, 0.8	1.0, 1.2, 1.5	
RV *Polarstern*, Norway	Polar	June–July 2018	Measured		0.1–1.0	Between 2 and 5	Kecorius et al. (2019)
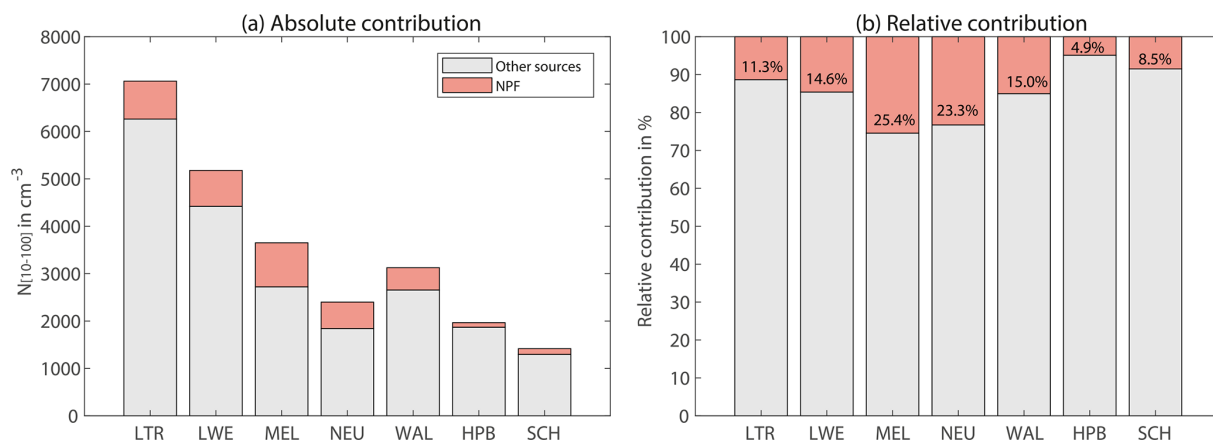
Figure 10. The absolute and relative contribution of NPF (red) to UFPs (N_{10-100}) for GUAN sites.
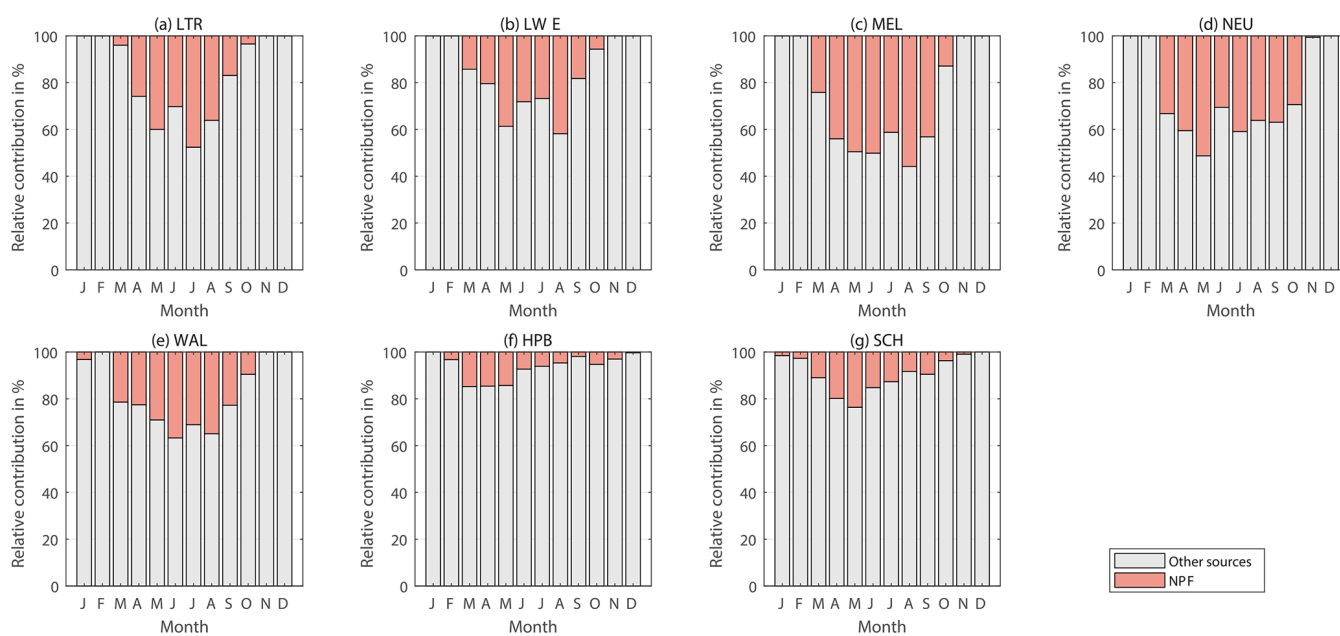
Figure 11. The monthly distribution of the relative contribution of NPF to UFPs (N_{10-100}) in the seven GUAN sites.

(UB) to high Alpine (HA). The NPF occurrence frequencies show significant differences with respect to site categories, while the NPF occurrence frequencies at the sites in the same category were found to be similar. Regional background (RB) sites had the highest NPF occurrence frequency, with an average value of about 19 %, followed by UB sites with an average of 15 %. NPF events were observed on 7 % of days at low-mountain-range (LMT) sites and only 3 % of days at the HA site ZSF. The NPF occurrence frequencies at GUAN sites in this work were found to be in the range of the occurrence frequency at other sites in central Europe reported in previous studies.

The annual mean growth rate for particle sizes of 10–25 nm (GR_{10-25}) varied from 3.7 to 4.7 nm h^{-1}, with minor differences among sites. The annual formation rate J_{10-25}

ranged from 0.4 to 2.9 cm^{-3} s^{-1} and increased with a higher degree of anthropogenic emissions, implying the crucial role of anthropogenic precursors in NPF. GR_{10-25} values for GUAN sites fall within the range of those reported in previous European studies. Obvious seasonal patterns of GR_{10-25} and J_{10-25} were observed, with the highest in summer and the lowest in winter for UB and RB sites. Different seasonal patterns for the three mountainous sites were observed, with the maximum in J_{10-25} being reached in spring. Most NPF events started between 07:30 and 09:00 in solar time. An earlier start time was found in summer due to earlier sunrise times. The three mountainous sites had the latest start time around 09:00. The two UB sites, LTR and LWE, had the earliest start time at around 07:30, while BOS and the three RB sites had a start time at around 08:30. The difference in

Table 4. The enhancement of the extinction coefficient at 550 nm ($\sigma_{\text{ext, 550 nm}}$) by NPF for GUAN sites. The bold numbers denote the statistically significant results with $\alpha = 0.05$.

Site category	Site	$\sigma_{\text{ext, 550 nm}}$ enhancement
UB	LTR	1.0
	LWE	1.0
	BOS	1.2
RB	MEL	1.1
	NEU	**1.4**
	WAL	1.0
LMT	HPB	**1.8**
	SCH	**1.6**
HA	ZSF	**1.9**

start time among sites mainly stems from the different diurnal variations in precursor concentration and CS.

The impact of NPF on ultrafine particles (UFPs), cloud condensation nuclei (CCN), and radiative forcing was quantitatively evaluated and discussed. Over the entire observation period, the contribution of NPF to UFPs was about 13 %, 21 %, and 7 % for the UB, RB, and LMT sites, respectively. The enhancement of CCN number concentration on NPF days was found to be the highest and the most significant in mountainous sites. Similarly, the enhancement of the aerosol extinction coefficient at 550 nm ($\sigma_{\text{ext, 550 nm}}$) on NPF days was 1.4, 1.8, 1.6, and 1.9 at the sites NEU, HPB, SCH, and ZSF, respectively, while no statistically significant contributions were observed for the other sites. These findings underscore the importance of considering the local environments of NPF when assessing its potential impact on regional climate in models. They also emphasize the usefulness of a long-term aerosol measurement network with multiple sites for understanding the variation in NPF features and their influencing factors over a regional scale.

Author contributions. AW, NM, WB, MH, and JS designed the research. JS, YY, and NM conducted the data analysis with help from VMK and MK. KaW, MM, TT, HF, BB, LR, CC, ME, RS, KlW, FM, MS, OB, and BH conducted the measurements. JS and NM wrote the paper with input from all co-authors.

References

Asmi, E., Kivekas, N., Kerminen, V.-M., Komppula, M., Hyvarinen, A.-P., Hatakka, J., Viisanen, Y., and Lihavainen, H.: Secondary new particle formation in Northern Finland Pallas site between the years 2000 and 2010, Atmos. Chem. Phys., 11, 12959–12972, https://doi.org/10.5194/acp-11-12959-2011, 2011.

Baalbaki, R., Pikridas, M., Jokinen, T., Laurila, T., Dada, L., Bezantakos, S., Ahonen, L., Neitola, K., Maisser, A., Bimenyimana, E., Christodoulou, A., Unga, F., Savvides, C., Lehtipalo, K., Kangasluoma, J., Biskos, G., Petäjä, T., Kerminen, V. M., Sciare, J., and Kulmala, M.: Towards understanding the characteris-

tics of new particle formation in the Eastern Mediterranean, Atmos. Chem. Phys., 21, 9223–9251, https://doi.org/10.5194/acp-21-9223-2021, 2021.

Bianchi, F., Tröstl, J., Junninen, H., Frege, C., Henne, S., Hoyle, C.-R., Molteni, U., Herrmann, E., Adamov, A., Bukowiecki, N., Chen, X., Duplissy, J., Gysel, M., Hutterli, M., Kangasluoma, J., Kontkanen, J., Kürten, A., Manninen, H. E., Münch, S., Peräkylä, O., Petäjä, T., Rondo, L., Williamson, C., Weingartner, E., Curtius, J., Worsnop, D. R., Kulmala, M., Dommen, J., and Baltensperger, U.: New particle formation in the free troposphere: A question of chemistry and timing, Science, 352, 1109–1112, https://doi.org/10.1126/science.aad5456, 2016.

Birmili, W., Weinhold, K., Rasch, F., Sonntag, A., Sun, J., Merkel, M., Wiedensohler, A., Bastian, S., Schladitz, A., Löschau, G., Cyrys, J., Pitz, M., Gu, J., Kusch, T., Flentje, H., Quass, U., Kaminski, H., Kuhlbusch, T. A. J., Meinhardt, F., Schwerin, A., Bath, O., Ries, L., Gerwig, H., Wirtz, K., and Fiebig, M.: Long-term observations of tropospheric particle number size distributions and equivalent black carbon mass concentrations in the German Ultrafine Aerosol Network (GUAN), Earth Syst. Sci. Data, 8, 355–382, https://doi.org/10.5194/essd-8-355-2016, 2016.

Birmili, W. and Wiedensohler, A.: New particle formation in the continental boundary layer: Meteorological and gas phase parameter influence, Geophys. Res. Lett., 27, 3325–3328, https://doi.org/10.1029/1999GL011221, 2000.

Boulon, J., Sellegri, K., Hervo, M., Picard, D., Pichon, J.-M., Fréville, P., and Laj, P.: Investigation of nucleation events vertical extent: a long term study at two different altitude sites, Atmos. Chem. Phys., 11, 5625–5639, https://doi.org/10.5194/acp-11-5625-2011, 2011.

Bousiotis, D., Dall'Osto, M., Beddows, D.-C.-S., Pope, F.-D., and Harrison, R.-M.: Analysis of new particle formation (NPF) events at nearby rural, urban background and urban roadside sites, Atmos. Chem. Phys., 19, 5679–5694, https://doi.org/10.5194/acp-19-5679-2019, 2019.

Bousiotis, D., Brean, J., Pope, F.-D., Dall'Osto, M., Querol, X., Alastuey, A., Perez, N., Petaja, T., Massling, A., Nojgaard, J. K., Nordstrom, C., Kouvarakis, G., Vratolis, S., Eleftheriadis, K., Niemi, J.-V., Portin, H., Wiedensohler, A., Weinhold, K., Merkel, M., Tuch, T., and Harrison, R.-M.: The effect of meteorological conditions and atmospheric composition in the occurrence and development of new particle formation (NPF) events in Europe, Atmos. Chem. Phys., 21, 3345–3370, https://doi.org/10.5194/acp-21-3345-2021, 2021a.

Bousiotis, D., Pope, F.-D., Beddows, D.-C.-S., Dall'Osto, M., Massling, A., Nojgaard, J.-K., Nordstrom, C., Niemi, J.-V., Portin, H., Petaja, T., Perez, N., Alastuey, A., Querol, X., Kouvarakis, G., Mihalopoulos, N., Vratolis, S., Eleftheriadis, K., Wiedensohler, A., Weinhold, K., Merkel, M., Tuch, T., and Harrison, R.-M.: A phenomenology of new particle formation (NPF) at 13 European sites, Atmos. Chem. Phys., 21, 11905–11925, https://doi.org/10.5194/acp-21-11905-2021, 2021b.

Boy, M. and Kulmala, M.: Nucleation events in the continental boundary layer: Influence of physical and meteorological parameters, Atmos. Chem. Phys., 2, 1–16, https://doi.org/10.5194/acp-2-1-2002, 2002.

Brines, M., Dall'Osto, M., Beddows, D.-C.-S., Harrison, R.-M., Gómez-Moreno, F., Núñez, L., Artíñano, B., Costabile, F., Gobbi, G.-P., Salimi, F., Morawska, L., Sioutas, C., and Querol,

X.: Traffic and nucleation events as main sources of ultrafine particles in high-insolation developed world cities, Atmos. Chem. Phys., 15, 5929–5945, https://doi.org/10.5194/acp-15-5929-2015, 2015.

Cai, R., Yang, D., Fu, Y., Wang, X., Li, X., Ma, Y., Hao, J., Zheng, J., and Jiang, J.: Aerosol surface area concentration: a governing factor in new particle formation in Beijing, Atmos. Chem. Phys., 17, 12327–12340, https://doi.org/10.5194/acp-17-12327-2017, 2017.

Casquero-Vera, J.-A., Lyamani, H., Dada, L., Hakala, S., Paasonen, P., Román, R., Fraile, R., Petäjä, T., Olmo-Reyes, F.-J., and Alados-Arboledas, L.: New particle formation at urban and high-altitude remote sites in the south-eastern Iberian Peninsula, Atmos. Chem. Phys., 20, 14253–14271, https://doi.org/10.5194/acp-20-14253-2020, 2020.

Collaud-Coen, M., Andrews, E., Aliaga, D., Andrade, M., Angelov, H., Bukowiecki, N., Ealo, M., Fialho, P., Flentje, H., Hallar, A. G., Hooda, R., Kalapov, I., Krejci, R., Lin, N. H., Marinoni, A., Ming, J., Nguyen, N. A., Pandolfi, M., Pont, V., Ries, L., Rodríguez, S., Schauer, G., Sellegri, K., Sharma, S., Sun, J., Tunved, P., Velasquez, P., and Ruffieux, D.: Identification of topographic features influencing aerosol observations at high altitude stations, Atmos. Chem. Phys., 18, 12289–12313, https://doi.org/10.5194/acp-18-12289-2018, 2018.

Costabile, F., Birmili, W., Klose, S., Tuch, T., Wehner, B., Wiedensohler, A., Franck, U., König, K., and Sonntag, A.: Spatio-temporal variability and principal components of the particle number size distribution in an urban atmosphere, Atmos. Chem. Phys., 9, 3163–3195, https://doi.org/10.5194/acp-9-3163-2009, 2009.

Dada, L., Paasonen, P., Nieminen, T., Buenrostro Mazon, S., Kontkanen, J., Peräkylä, O., Lehtipalo, K., Hussein, T., Petäjä, T., Kerminen, V.-M., Bäck, J., and Kulmala, M.: Long-term analysis of clear-sky new particle formation events and non-events in Hyytiälä, Atmos. Chem. Phys., 17, 6227–6241, https://doi.org/10.5194/acp-17-6227-2017, 2017.

Dada, L., Ylivinkka, I., Baalbaki, R., Li, C., Guo, Y., Yan, C., Yao, L., Sarnela, N., Jokinen, T., Daellenbach, K.-R., Yin, R., Deng, C., Chu, B., Nieminen, T., Wang, Y., Lin, Z., Thakur, R. C., Kontkanen, J., Stolzenburg, D., Sipilä, M., Hussein, T., Paasonen, P., Bianchi, F., Salma, I., Weidinger, T., Pikridas, M., Sciare, J., Jiang, J., Liu, Y., Petäjä, T., Kerminen, V.-M., and Kulmala, M.: Sources and sinks driving sulfuric acid concentrations in contrasting environments: implications on proxy calculations, Atmos. Chem. Phys., 20, 11747–11766, https://doi.org/10.5194/acp-20-11747-2020, 2020.

Dall'Osto, M., Beddows, D.-C.-S., Asmi, A., Poulain, L., Hao, L., Freney, E., Allan, J.-D., Canagaratna, M., Crippa, M., Bianchi, F., de Leeuw, G., Eriksson, A., Swietlicki, E., Hansson, H.-C., Henzing, J.-S., Granier, C., Zemankova, K., Laj, P., Onasch, T., Prevot, A., Putaud, J.-P., Sellegri, K., Vidal, M., Virtanen, A., Simo, R., Worsnop, D., O'Dowd, C., Kulmala, M., and Harrison, R.-M.: Novel insights on new particle formation derived from a pan-European observing system, Sci. Rep., 8, 1482, https://doi.org/10.1038/s41598-017-17343-9, 2018.

Dal Maso, M., Kulmala, M., Riipinen, I., Wagner, R., Hussein, T., Aalto, P.-P., and Lehtinen, K.-E.: Formation and growth of fresh atmospheric aerosols: eight years of aerosol size distribution data

from SMEAR II, Hyytiala, Finland, Boreal Environ. Res., 10, 323–336, 2005.

Dameto de España, C., Wonaschütz, A., Steiner, G., Rosati, B., Demattio, A., Schuh, H., and Hitzenberger, R.: Long-term quantitative field study of New Particle Formation (NPF) events as a source of Cloud Condensation Nuclei (CCN) in the urban background of Vienna, Atmos. Environ., 164, 289–298, https://doi.org/10.1016/j.atmosenv.2017.06.001, 2017.

Ehn, M., Thornton, J.-A., Kleist, E., Sipila, M., Junninen, H., Pullinen, I., Springer, M., Rubach, F., Tillmann, R., Lee, B., Lopez-Hilfiker, F., Andres, S., Acir, I.-H., Rissanen, M., Jokinen, T., Schobesberger, S., Kangasluoma, J., Kontkanen, J., Nieminen, T., Kurten, T., Nielsen, L.-B., Jorgensen, S., Kjaergaard, H.-G., Canagaratna, M., Dal Maso, M., Berndt, T., Petaja, T., Wahner, A., Kerminen, V.-M., Kulmala, M., Worsnop, D.-R., Wildt, J., and Mentel, T.-F.: A large source of low-volatility secondary organic aerosol, Nature, 506, 476–479, https://doi.org/10.1038/nature13032, 2014.

Flentje, H., Claude, H., Elste, T., Gilge, S., Köhler, U., Plass-Dülmer, C., Steinbrecht, W., Thomas, W., Werner, A., and Fricke, W.: The Eyjafjallajökull eruption in April 2010 – detection of volcanic plume using in-situ measurements, ozone sondes and lidar-ceilometer profiles, Atmos. Chem. Phys., 10, 10085–10092, https://doi.org/10.5194/acp-10-10085-2010, 2010.

Größ, J., Hamed, A., Sonntag, A., Spindler, G., Manninen, H.-E., Nieminen, T., Kulmala, M., Hõrrak, U., Plass-Dülmer, C., Wiedensohler, A., and Birmili, W.: Atmospheric new particle formation at the research station Melpitz, Germany: connection with gaseous precursors and meteorological parameters, Atmos. Chem. Phys., 18, 1835–1861, https://doi.org/10.5194/acp-18-1835-2018, 2018.

Hanson, D.-R., Bier, I., Panta, B., Jen, C.-N., and McMurry, P.-H.: Computational Fluid Dynamics Studies of a Flow Reactor: Free Energies of Clusters of Sulfuric Acid with NH3 or Dimethyl Amine, J. Phys. Chem. A, 121, 3976–3990, https://doi.org/10.1021/acs.jpca.7b00252, 2017.

Herrmann, E., Weingartner, E., Henne, S., Vuilleumier, L., Bukowiecki, N., Steinbacher, M., Conen, F., Collaud Coen, M., Hammer, E., Jurányi, Z., Baltensperger, U., and Gysel, M.: Analysis of long-term aerosol size distribution data from Jungfraujoch with emphasis on free tropospheric conditions, cloud influence, and air mass transport, Geophys. Res., 120, 9459–9480, https://doi.org/10.1002/2015JD023660, 2015.

Hirshorn, N.-S., Zuromski, L.-M., Rapp, C., McCubbin, I., Carrillo-Cardenas, G., Yu, F., and Hallar, A.-G.: Seasonal significance of new particle formation impacts on cloud condensation nuclei at a mountaintop location, Atmos. Chem. Phys., 22, 15909–15924, https://doi.org/10.5194/acp-22-15909-2022, 2022.

Hofman, J., Staelens, J., Cordell, R., Stroobants, C., Zikova, N., Hama, S.-M.-L., Wyche, K.-P., Kos, G.-P.-A., Van der Zee, S., Smallbone, K.-L., Weijers, E.-P., Monks, P.-S., and Roekens, E.: Ultrafine particles in four European urban environments: Results from a new continuous long-term monitoring network, Atmos. Environ., 136, 68–81, https://doi.org/10.1016/j.atmosenv.2016.04.010, 2016.

Joutsensaari, J., Ozon, M., Nieminen, T., Mikkonen, S., Lahivaara, T., Decesari, S., Facchini, M.-C., Laaksonen, A., and Lehtinen, K.-E.-J.: Identification of new particle formation events

with deep learning, Atmos. Chem. Phys., 18, 9597–9615, https://doi.org/10.5194/acp-18-9597-2018, 2018.

Kalkavouras, P., Bougiatioti, A., Kalivitis, N., Stavroulas, I., Tombrou, M., Nenes, A., and Mihalopoulos, N.: Regional new particle formation as modulators of cloud condensation nuclei and cloud droplet number in the eastern Mediterranean, Atmos. Chem. Phys., 19, 6185–6203, https://doi.org/10.5194/acp-19-6185-2019, 2019.

Kalkavouras, P., Bougiatioti, A., Grivas, G., Stavroulas, I., Kalivitis, N., Liakakou, E., Gerasopoulos, E., Pilinis, C., and Mihalopoulos, N.: On the regional aspects of new particle formation in the Eastern Mediterranean: A comparative study between a background and an urban site based on long term observations, Atmos. Res., 239, 104911, https://doi.org/10.1016/j.atmosres.2020.104911, 2020.

Kecorius, S., Vogl, T., Paasonen, P., Lampilahti, J., Rothenberg, D., Wex, H., Zeppenfeld, S., van Pinxteren, M., Hartmann, M., Henning, S., Gong, X., Welti, A., Kulmala, M., Stratmann, F., Herrmann, H., and Wiedensohler, A.: New particle formation and its effect on cloud condensation nuclei abundance in the summer Arctic: a case study in the Fram Strait and Barents Sea, Atmos. Chem. Phys., 19, 14339–14364, https://doi.org/10.5194/acp-19-14339-2019, 2019.

Kerminen, V.-M., Pirjola, L., and Kulmala, M.: How significantly does coagulational scavenging limit atmospheric particle production?, J. Geophys. Res.-Atmos., 106, 24119–24125, https://doi.org/10.1029/2001jd000322, 2001.

Kerminen, V.-M., Paramonov, M., Anttila, T., Riipinen, I., Fountoukis, C., Korhonen, H., Asmi, E., Laakso, L., Lihavainen, H., Swietlicki, E., Svenningsson, B., Asmi, A., Pandis, S.-N., Kulmala, M., and Petäjä, T.: Cloud condensation nuclei production associated with atmospheric nucleation: a synthesis based on existing literature and new results, Atmos. Chem. Phys., 12, 12037–12059, https://doi.org/10.5194/acp-12-12037-2012, 2012.

Kerminen, V.-M., Chen, X.-M., Vakkari, V., Petaja, T., Kulmala, M., and Bianchi, F.: Atmospheric new particle formation and growth: review of field observations, Environ. Res. Lett., 13, 103003, https://doi.org/10.1088/1748-9326/aadf3c, 2018.

Kulmala, M., Petäjä, T., Nieminen, T., Sipilä, M., Manninen, H.-E., Lehtipalo, K., Dal Maso, M., Aalto, P.-P., Junninen, H., Paasonen, P., Riipinen, I., Lehtinen, K.-E.-J., Laaksonen, A., and Kerminen, V.-M.: Measurement of the nucleation of atmospheric aerosol particles, Nat. Protocol., 7, 1651–1667, https://doi.org/10.1038/nprot.2012.091, 2012.

Kulmala, M., Petaja, T., Ehn, M., Thornton, J., Sipila, M., Worsnop, D.-R., and Kerminen, V.-M.: Chemistry of Atmospheric Nucleation: On the Recent Advances on Precursor Characterization and Atmospheric Cluster Composition in Connection with Atmospheric New Particle Formation, Annu. Rev. Phys. Chem., 65, 21–37, https://doi.org/10.1146/annurev-physchem-040412-110014, 2014.

Kulmala, M., Cai, R., Stolzenburg, D., Zhou, Y., Dada, L., Guo, Y., Yan, C., Petäjä, T., Jiang, J., and Kerminen, V.-M.: The contribution of new particle formation and subsequent growth to haze formation, Environ. Sci.-Atmos., 2, 352–361, https://doi.org/10.1039/D1EA00096A, 2022a.

Kulmala, M., Junninen, H., Dada, L., Salma, I., Weidinger, T., Thén, W., Vörösmarty, M., Komsaare, K., Stolzenburg, D., Cai, R., Yan, C., Li, X., Deng, C., Jiang, J., Petäjä, T., Niem-

inen, T., and Kerminen, V.-M.: Quiet New Particle Formation in the Atmosphere, Front. Environ. Sci., 10, 912385, https://doi.org/10.3389/fenvs.2022.912385, 2022b.

Kulmala, M., Cai, R.-L., Ezhova, E., Deng, C.-J., Stolzenburg, D., Dada, L., Guo, Y.-S., Yan, C., Perakyla, O., Lintunen, A., Nieminen, T., Kokkonen, T.-V., Sarnela, N., Petaja, T., and Kerminen, V.-M.: Direct link between the characteristics of atmospheric new particle formation and Continental Biosphere-Atmosphere-Cloud-Climate (COBACC) feedback loop, Boreal Environ. Res., 28, 1–13, 2023.

Kürten, A., Bergen, A., Heinritzi, M., Leiminger, M., Lorenz, V., Piel, F., Simon, M., Sitals, R., Wagner, A.-C., and Curtius, J.: Observation of new particle formation and measurement of sulfuric acid, ammonia, amines and highly oxidized organic molecules at a rural site in central Germany, Atmos. Chem. Phys., 16, 12793–12813, https://doi.org/10.5194/acp-16-12793-2016, 2016.

Kürten, A., Li, C., Bianchi, F., Curtius, J., Dias, A., Donahue, N.-M., Duplissy, J., Flagan, R.-C., Hakala, J., Jokinen, T., Kirkby, J., Kulmala, M., Laaksonen, A., Lehtipalo, K., Makhmutov, V., Onnela, A., Rissanen, M.-P., Simon, M., Sipilä, M., Stozhkov, Y., Tröstl, J., Ye, P., and McMurry, P.-H.: New particle formation in the sulfuric acid–dimethylamine–water system: reevaluation of CLOUD chamber measurements and comparison to an aerosol nucleation and growth model, Atmos. Chem. Phys., 18, 845–863, https://doi.org/10.5194/acp-18-845-2018, 2018.

Laaksonen, A., Kulmala, M., O'Dowd, C.-D., Joutsensaari, J., Vaattovaara, P., Mikkonen, S., Lehtinen, K.-E.-J., Sogacheva, L., Dal Maso, M., Aalto, P., Petäjä, T., Sogachev, A., Yoon, Y.-J., Lihavainen, H., Nilsson, D., Facchini, M.-C., Cavalli, F., Fuzzi, S., Hoffmann, T., Arnold, F., Hanke, M., Sellegri, K., Umann, B., Junkermann, W., Coe, H., Allan, J.-D., Alfarra, M.-R., Worsnop, D.-R., Riekkola, M.-L., Hyötyläinen, T., and Viisanen, Y.: The role of VOC oxidation products in continental new particle formation, Atmos. Chem. Phys., 8, 2657–2665, https://doi.org/10.5194/acp-8-2657-2008, 2008.

Lee, H., Lee, K., Lunder, C.-R., Krejci, R., Aas, W., Park, J., Park, K.-T., Lee, B.-Y., Yoon, Y.-J., and Park, K.: Atmospheric new particle formation characteristics in the Arctic as measured at Mount Zeppelin, Svalbard, from 2016 to 2018, Atmos. Chem. Phys., 20, 13425–13441, https://doi.org/10.5194/acp-20-13425-2020, 2020.

Lee, S.-H., Gordon, H., Yu, H., Lehtipalo, K., Haley, R., Li, Y., and Zhang, R.: New Particle Formation in the Atmosphere: From Molecular Clusters to Global Climate, Geophys. Res., 124, 7098–7146, https://doi.org/10.1029/2018JD029356, 2019.

Li, X., Chee, S., Hao, J., Abbatt, J.-P.-D., Jiang, J., and Smith, J.-N.: Relative humidity effect on the formation of highly oxidized molecules and new particles during monoterpene oxidation, Atmos. Chem. Phys., 19, 1555–1570, https://doi.org/10.5194/acp-19-1555-2019, 2019.

Ma, N. and Birmili, W.: Estimating the contribution of photochemical particle formation to ultrafine particle number averages in an urban atmosphere, Sci. Total Environ., 512/513, 154–166, https://doi.org/10.1016/j.scitotenv.2015.01.009, 2015.

Mäkelä, J.-M., Aalto, P., Jokinen, V., Pohja, T., Nissinen, A., Palmroth, S., Markkanen, T., Seitsonen, K., Lihavainen, H., and Kulmala, M.: Observations of ultrafine aerosol particle formation and growth in boreal forest, Geophys. Res. Lett., 24, 1219–1222, https://doi.org/10.1029/97GL00920, 1997.

Manninen, H.-E., Nieminen, T., Asmi, E., Gagné, S., Häkkinen, S., Lehtipalo, K., Aalto, P., Vana, M., Mirme, A., Mirme, S., Hõrrak, U., Plass-Dülmer, C., Stange, G., Kiss, G., Hoffer, A., Törő, N., Moerman, M., Henzing, B., de Leeuw, G., Brinkenberg, M., Kouvarakis, G.-N., Bougiatioti, A., Mihalopoulos, N., O'Dowd, C., Ceburnis, D., Arneth, A., Svenningsson, B., Swietlicki, E., Tarozzi, L., Decesari, S., Facchini, M.-C., Birmili, W., Sonntag, A., Wiedensohler, A., Boulon, J., Sellegri, K., Laj, P., Gysel, M., Bukowiecki, N., Weingartner, E., Wehrle, G., Laaksonen, A., Hamed, A., Joutsensaari, J., Petäjä, T., Kerminen, V.-M., and Kulmala, M.: EUCAARI ion spectrometer measurements at 12 European sites – analysis of new particle formation events, Atmos. Chem. Phys., 10, 7907–7927, https://doi.org/10.5194/acp-10-7907-2010, 2010.

Mie, G.: Articles on the optical characteristics of turbid tubes, especially colloidal metal solutions, Ann. Phys., 25, 377–445, https://doi.org/10.1002/andp.19083300302, 1908.

Németh, Z. and Salma, I.: Spatial extension of nucleating air masses in the Carpathian Basin, Atmos. Chem. Phys., 14, 8841–8848, https://doi.org/10.5194/acp-14-8841-2014, 2014.

Németh, Z., Rosati, B., Zíková, N., Salma, I., Bozó, L., Dameto de España, C., Schwarz, J., Ždímal, V., and Wonaschütz, A.: Comparison of atmospheric new particle formation events in three Central European cities, Atmos. Environ., 178, 191–197, https://doi.org/10.1016/j.atmosenv.2018.01.035, 2018.

Nieminen, T., Asmi, A., Dal Maso, M., Aalto, P., Keronen, P., Petaja, T., Kulmala, M., and Kerminen, V.-M.: Trends in atmospheric new-particle formation: 16 years of observations in a boreal-forest environment, Boreal Environ. Res., 19, 191–214, 2014.

Nieminen, T., Kerminen, V.-M., Petaja, T., Aalto, P.-P., Arshinov, M., Asmi, E., Baltensperger, U., Beddows, D.-C.-S., Beukes, J.-P., Collins, D., Ding, A.-J., Harrison, R.-M., Henzing, B., Hooda, R., Hu, M., Horrak, U., Kivekas, N., Komsaare, K., Krejci, R., Kristensson, A., Laakso, L., Laaksonen, A., Leaitch, W.-R., Lihavainen, H., Mihalopoulos, N., Nemeth, Z., Nie, W., O'Dowd, C., Salma, I., Sellegri, K., Svenningsson, B., Swietlicki, E., Tunved, P., Ulevicius, V., Vakkari, V., Vana, M., Wiedensohler, A., Wu, Z.-J., Virtanen, A., and Kulmala, M.: Global analysis of continental boundary layer new particle formation based on long-term measurements, Atmos. Chem. Phys., 18, 14737–14756, https://doi.org/10.5194/acp-18-14737-2018, 2018.

O'Dowd, C.-D., Geever, M., and Hill, M.-K.: New particle formation: Nucleation rates and spatial scales in the clean marine coastal environment, Geophys. Res. Lett., 25, 1661–1664, https://doi.org/10.1029/98gl01005, 1998.

Petäjä, T., Mauldin, I.-R.-L., Kosciuch, E., McGrath, J., Nieminen, T., Paasonen, P., Boy, M., Adamov, A., Kotiaho, T., and Kulmala, M.: Sulfuric acid and OH concentrations in a boreal forest site, Atmos. Chem. Phys., 9, 7435–7448, https://doi.org/10.5194/acp-9-7435-2009, 2009.

Pfeifer, S., Birmili, W., Schladitz, A., Müller, T., Nowak, A., and Wiedensohler, A.: A fast and easy-to-implement inversion algorithm for mobility particle size spectrometers considering particle number size distribution information outside of the detection range, Atmos. Meas. Tech., 7, 95–105, https://doi.org/10.5194/amt-7-95-2014, 2014.

Plauskaite, K., Ulevicius, V., Spirkauskaite, N., Bycenkiene, S., Zielinski, T., Petelski, T., and Ponczkowska, A.: Observations

of new particle formation events in the south-eastern Baltic Sea, Oceanologia, 52, 53–75, https://doi.org/10.5697/oc.52-1.053, 2010.

Qi, X.-M., Ding, A.-J., Roldin, P., Xu, Z.-N., Zhou, P.-T., Sarnela, N., Nie, W., Huang, X., Rusanen, A., Ehn, M., Rissanen, M.-P., Petaja, T., Kulmala, M., and Boy, M.: Modelling studies of HOMs and their contributions to new particle formation and growth: comparison of boreal forest in Finland and a polluted environment in China, Atmos. Chem. Phys., 18, 11779–11791, https://doi.org/10.5194/acp-18-11779-2018, 2018.

Rejano, F., Titos, G., Casquero-Vera, J.-A., Lyamani, H., Andrews, E., Sheridan, P., Cazorla, A., Castillo, S., Alados-Arboledas, L., and Olmo, F.-J.: Activation properties of aerosol particles as cloud condensation nuclei at urban and high-altitude remote sites in southern Europe, Sci. Total Environ., 762, 143100, https://doi.org/10.1016/j.scitotenv.2020.143100, 2021.

Ren, J.-Y., Chen, L., Fan, T.-Y., Liu, J.-Y., Jiang, S.-H., and Zhang, F.: The NPF Effect on CCN Number Concentrations: A Review and Re-Evaluation of Observations From 35 Sites Worldwide, Geophys. Res. Lett., 48, e2021GL095190, https://doi.org/10.1029/2021gl095190, 2021.

Rose, C., Sellegri, K., Moreno, I., Velarde, F., Ramonet, M., Weinhold, K., Krejci, R., Andrade, M., Wiedensohler, A., Ginot, P., and Laj, P.: CCN production by new particle formation in the free troposphere, Atmos. Chem. Phys., 17, 1529–1541, https://doi.org/10.5194/acp-17-1529-2017, 2017.

Salma, I. and Németh, Z.: Dynamic and timing properties of new aerosol particle formation and consecutive growth events, Atmos. Chem. Phys., 19, 5835–5852, https://doi.org/10.5194/acp-19-5835-2019, 2019.

Salma, I., Németh, Z., Kerminen, V.-M., Aalto, P., Nieminen, T., Weidinger, T., Molnár, Á., Imre, K., and Kulmala, M.: Regional effect on urban atmospheric nucleation, Atmos. Chem. Phys., 16, 8715–8728, https://doi.org/10.5194/acp-16-8715-2016, 2016.

Salma, I., Varga, V., and Németh, Z.: Quantification of an atmospheric nucleation and growth process as a single source of aerosol particles in a city, Atmos. Chem. Phys., 17, 15007–15017, https://doi.org/10.5194/acp-17-15007-2017, 2017.

Salvador, P., Barreiro, M., Gomez-Moreno, F.-J., Alonso-Blanco, E., and Artinano, B.: Synoptic classification of meteorological patterns and their impact on air pollution episodes and new particle formation processes in a south European air basin, Atmos. Environ., 245, 118016, https://doi.org/10.1016/j.atmosenv.2020.118016, 2021.

Sebastian, M., Kompalli, S.-K., Kumar, V.-A., Jose, S., Babu, S.-S., Pandithurai, G., Singh, S., Hooda, R.-K., Soni, V.-K., Pierce, J.-R., Vakkari, V., Asmi, E., Westervelt, D.-M., Hyvarinen, A.-P., and Kanawade, V.-P.: Observations of particle number size distributions and new particle formation in six Indian locations, Atmos. Chem. Phys., 22, 4491–4508, https://doi.org/10.5194/acp-22-4491-2022, 2022.

Seinfeld, J.-H., Pandis, S.-N., and Noone, K.: Atmospheric Chemistry and Physics: From Air Pollution to Climate Change, Phys. Today, 51, 88–90, https://doi.org/10.1063/1.882420, 1998.

Sellegri, K., Rose, C., Marinoni, A., Lupi, A., Wiedensohler, A., Andrade, M., Bonasoni, P., and Laj, P.: New Particle Formation: A Review of Ground-Based Observations at Mountain Research Stations, Atmosphere, 10, 493, https://doi.org/10.3390/atmos10090493, 2019.

Shen, X., Sun, J., Zhang, X., Kivekäs, N., Zhang, Y., Wang, T., Zhang, X., Yang, Y., Wang, D., Zhao, Y., and Qin, D.: Particle Climatology in Central East China Retrieved from Measurements in Planetary Boundary Layer and in Free Troposphere at a 1500-m-High Mountaintop Site, Aerosol Air Qual. Res., 16, 689–701, https://doi.org/10.4209/aaqr.2015.02.0070, 2016.

Shen, X.-J., Sun, J.-Y., Zhang, Y.-M., Wehner, B., Nowak, A., Tuch, T., Zhang, X.-C., Wang, T.-T., Zhou, H.-G., Zhang, X.-L., Dong, F., Birmili, W., and Wiedensohler, A.: First long-term study of particle number size distributions and new particle formation events of regional aerosol in the North China Plain, Atmos. Chem. Phys., 11, 1565–1580, https://doi.org/10.5194/acp-11-1565-2011, 2011.

Sihto, S.-L., Mikkilä, J., Vanhanen, J., Ehn, M., Liao, L., Lehtipalo, K., Aalto, P.-P., Duplissy, J., Petäjä, T., Kerminen, V.-M., Boy, M., and Kulmala, M.: Seasonal variation of CCN concentrations and aerosol activation properties in boreal forest, Atmos. Chem. Phys., 11, 13269–13285, https://doi.org/10.5194/acp-11-13269-2011, 2011.

Smejkalova, A.-H., Zikova, N., Zdimal, V., Placha, H., and Bitter, M.: Atmospheric aerosol growth rates at different background station types, Environ. Sci. Pollut. Res., 28, 13352–13364, https://doi.org/10.1007/s11356-020-11424-5, 2021.

Spindler, G., Grüner, A., Müller, K., Schlimper, S., and Herrmann, H.: Long-term size-segregated particle (PM_{10}, $PM_{2.5}$, PM_1) characterization study at Melpitz influence of air mass inflow, weather conditions and season, J. Atmos. Chem., 70, 165–195, https://doi.org/10.1007/s10874-013-9263-8, 2013.

Sun, J.: Particle number size distribution in GUAN from 2009 to 2013, Science Database, Zenodo [data set], https://doi.org/10.5281/zenodo.13235563, 2024.

Sun, J., Birmili, W., Hermann, M., Tuch, T., Weinhold, K., Spindler, G., Schladitz, A., Bastian, S., Löschau, G., Cyrys, J., Gu, J., Flentje, H., Briel, B., Asbach, C., Kaminski, H., Ries, L., Sohmer, R., Gerwig, H., Wirtz, K., Meinhardt, F., Schwerin, A., Bath, O., Ma, N., and Wiedensohler, A.: Variability of black carbon mass concentrations, sub-micrometer particle number concentrations and size distributions: results of the German Ultrafine Aerosol Network ranging from city street to High Alpine locations, Atmos. Environ., 202, 256–268, https://doi.org/10.1016/j.atmosenv.2018.12.029, 2019.

Sun, J., Birmili, W., Hermann, M., Tuch, T., Weinhold, K., Merkel, M., Rasch, F., Müller, T., Schladitz, A., Bastian, S., Löschau, G., Cyrys, J., Gu, J., Flentje, H., Briel, B., Asbach, C., Kaminski, H., Ries, L., Sohmer, R., Gerwig, H., Wirtz, K., Meinhardt, F., Schwerin, A., Bath, O., Ma, N., and Wiedensohler, A.: Decreasing trends of particle number and black carbon mass concentrations at 16 observational sites in Germany from 2009 to 2018, Atmos. Chem. Phys., 20, 7049–7068, https://doi.org/10.5194/acp-20-7049-2020, 2020.

Sun, J., Hermann, M., Yuan, Y., Birmili, W., Collaud Coen, M., Weinhold, K., Madueño, L., Poulain, L., Tuch, T., Ries, L., Sohmer, R., Couret, C., Frank, G., Brem, B. T., Gysel-Beer, M., Ma, N., and Wiedensohler, A.: Long-term trends of black carbon and particle number concentration in the lower free troposphere in Central Europe, Environ. Sci. Eur., 33, 47, https://doi.org/10.1186/s12302-021-00488-w, 2021.

Swietlicki, E., Hansson, H.-C., Hämeri, K., Svenningsson, B., Massling, A., McFiggans, G., McMurry, P., Petäjä, T., Tunved,

P., and Gysel, M.: Hygroscopic properties of submicrometer atmospheric aerosol particles measured with H-TDMA instruments in various environments – a review, Tellus B, 60, 432–469, https://doi.org/10.1111/j.1600-0889.2008.00350.x, 2008.

Tröstl, J., Herrmann, E., Frege, C., Bianchi, F., Molteni, U., Bukowiecki, N., Hoyle, C.-R., Steinbacher, M., Weingartner, E., Dommen, J., Gysel, M., and Baltensperger, U.: Contribution of new particle formation to the total aerosol concentration at the high-altitude site Jungfraujoch (3580 m a.s.l., Switzerland), Geophys. Res., 121, 11692–611711, https://doi.org/10.1002/2015JD024637, 2016.

Vaananen, R., Kyro, E.-M., Nieminen, T., Kivekas, N., Junninen, H., Virkkula, A., Dal Maso, M., Lihavainen, H., Viisanen, Y., Svenningsson, B., Holst, T., Arneth, A., Aalto, P.-P., Kulmala, M., and Kerminen, V.-M.: Analysis of particle size distribution changes between three measurement sites in northern Scandinavia, Atmos. Chem. Phys., 13, 11887–11903, https://doi.org/10.5194/acp-13-11887-2013, 2013.

Vana, M., Komsaare, K., Horrak, U., Mirme, S., Nieminen, T., Kontkanen, J., Manninen, H.-E., Petaja, T., Noe, S.-M., and Kulmala, M.: Characteristics of new-particle formation at three SMEAR stations, Boreal Environ. Res., 21, 345–362, 2016.

Wang, D., Guo, H., Cheung, K., and Gan, F.: Observation of nucleation mode particle burst and new particle formation events at an urban site in Hong Kong, Atmos. Environ., 99, 196–205, https://doi.org/10.1016/j.atmosenv.2014.09.074, 2014.

Wang, Z., Birmili, W., Hamed, A., Wehner, B., Spindler, G., Pei, X., Wu, Z., Cheng, Y., Su, H., and Wiedensohler, A.: Contributions of volatile and nonvolatile compounds (at 300 °C) to condensational growth of atmospheric nanoparticles: An assessment based on 8.5 years of observations at the Central Europe background site Melpitz, J. Geophys. Res.-Atmos., 122, 485–497, https://doi.org/10.1002/2016JD025581, 2017.

Wex, H., Neususs, C., Wendisch, M., Stratmann, F., Koziar, C., Keil, A., Wiedensohler, A., and Ebert, M.: Particle scattering, backscattering, and absorption coefficients: An in-situ closure and sensitivity study, J. Geophys. Res.-Atmos., 107, LAC 4-1–LAC 4-18, https://doi.org/10.1029/2000jd000234, 2002.

Wiedensohler, A.: An approximation of the bipolar charge distribution for particles in the submicron range, J. Aerosol Sci., 19, 387–389, 1988.

Wiedensohler, A., Birmili, W., Nowak, A., Sonntag, A., Weinhold, K., Merkel, M., Wehner, B., Tuch, T., Pfeifer, S., Fiebig, M., Fjäraa, A.-M., Asmi, E., Sellegri, K., Depuy, R., Venzac, H., Villani, P., Laj, P., Aalto, P., Ogren, J.-A., Swietlicki, E., Williams, P., Roldin, P., Quincey, P., Hüglin, C., Fierz-Schmidhauser, R., Gysel, M., Weingartner, E., Riccobono, F., Santos, S., Grüning, C., Faloon, K., Beddows, D., Harrison, R., Monahan, C., Jennings, S.-G., O'Dowd, C.-D., Marinoni, A., Horn, H.-G., Keck, L., Jiang, J., Scheckman, J., McMurry, P.-H., Deng, Z., Zhao, C.-S., Moerman, M., Henzing, B., de Leeuw, G., Löschau, G., and Bastian, S.: Mobility particle size spectrometers: harmonization of technical standards and data structure to facilitate high quality long-term observations of atmospheric particle number size distributions, Atmos. Meas. Tech., 5, 657–685, https://doi.org/10.5194/amt-5-657-2012, 2012.

Wiedensohler, A., Wiesner, A., Weinhold, K., Birmili, W., Hermann, M., Merkel, M., Müller, T., Pfeifer, S., Schmidt, A., Tuch, T., Velarde, F., Quincey, P., Seeger, S., and Nowak, A.: Mobility particle size spectrometers: Calibration procedures and measurement uncertainties, Aerosol Sci. Technol., 52, 146–164, https://doi.org/10.1080/02786826.2017.1387229, 2018.

Williamson, C.-J., Kupc, A., Axisa, D., Bilsback, K.-R., Bui, T., Campuzano-Jost, P., Dollner, M., Froyd, K.-D., Hodshire, A.-L., Jimenez, J.-L., Kodros, J.-K., Luo, G., Murphy, D.-M., Nault, B.-A., Ray, E.-A., Weinzierl, B., Wilson, J.-C., Yu, F.-Q., Yu, P.-F., Pierce, J.-R., and Brock, C.-A.: A large source of cloud condensation nuclei from new particle formation in the tropics, Nature, 574, 399–403, https://doi.org/10.1038/s41586-019-1638-9, 2019.

Wu, Z.-J., Poulain, L., Birmili, W., Größ, J., Niedermeier, N., Wang, Z.-B., Herrmann, H., and Wiedensohler, A.: Some insights into the condensing vapors driving new particle growth to CCN sizes on the basis of hygroscopicity measurements, Atmos. Chem. Phys., 15, 13071–13083, https://doi.org/10.5194/acp-15-13071-2015, 2015.

Yao, L., Garmash, O., Bianchi, F., Zheng, J., Yan, C., Kontkanen, J., Junninen, H., Mazon, S.-B., Ehn, M., Paasonen, P., Sipila, M., Wang, M.-Y., Wang, X.-K., Xiao, S., Chen, H.-F., Lu, Y.-Q., Zhang, B.-W., Wang, D.-F., Fu, Q.-Y., Geng, F.-H., Li,L., Wang, H.-L., Qiao, L.-P., Yang, X., Chen, J.-M., Kerminen, V.-M., Petaja, T., Worsnop, D.-R., Kulmala, M., and Wang, L.: Atmospheric new particle formation from sulfuric acid and amines in a Chinese megacity, Science, 361, 278–281, https://doi.org/10.1126/science.aao4839, 2018.

Yuan, Y., Ries, L., Petermeier, H., Trickl, T., Leuchner, M., Couret, C., Sohmer, R., Meinhardt, F., and Menzel, A.: On the diurnal, weekly, and seasonal cycles and annual trends in atmospheric CO_2 at Mount Zugspitze, Germany, during 1981–2016, Atmos. Chem. Phys., 19, 999–1012, https://doi.org/10.5194/acp-19-999-2019, 2019.